A Probabilistic Seismic Hazard Model for North Africa

Valerio Poggi[1,2] • **Julio Garcia-Peláez**[2] • **Richard Styron**[2] • **Marco Pagani**[2] •
Robin Gee[2]

⊠   Valerio Poggi, e-mail: vpoggi@inogs.org

1   Now at National Institute of Oceanography and Applied Geophysics (OGS), Udine, Italy

2   Global Earthquake Model Foundation (GEM), Pavia, Italy

Abstract African seismicity is predominantly localized along the East African Rift System (EARS), which is the major active tectonic feature of Sub-Saharan Africa. Besides the EARS, however, significant seismicity also occurs along a wide belt bounding the Mediterranean coastline. This tectonically active region extends discontinuously from Morocco to Egypt and its activity is controlled by the complex interaction between the Nubian and Eurasian plates, varying from transpression in the Atlas orogen in the west to transtension in the east. A record of large earthquake events is documented for the whole region, some of them causing moderate to severe levels of damage, mostly because of the high vulnerability of local buildings and structures, a condition which is still largely persistent in many areas.

Currently, a number of seismic hazard models exist at local and national scales for North Africa, developed within independent projects and created using inhomogeneous data sources and different processing techniques. Unfortunately, such diversity makes their direct comparison problematic, obscuring the differences in seismic hazard across neighbouring areas and preventing the development of comprehensive long-term risk mitigation strategies. In fact, the last effort to produce a homogenized model for the whole Africa continent dates back to the GSHAP project, which is almost twenty years old. The creation of a unique seismic hazard model for North Africa, uniform across countries, is therefore a main concern.

Since its inception, the Global Earthquake Model Foundation (GEM) is committed to the creation of a worldwide mosaic of high-quality, reproducible and openly

accessible seismic hazard models, uniformly represented using the format adopted by the OpenQuake engine (OQ), a state-of-the-art, free and open-source software package for seismic hazard and risk assessment. ~~In this manuscript we describe the work done for the creation of a new comprehensive PSHA model for North Africa, based on a combination of active faults from geodetical information and distributed seismicity from the observed earthquake record, modelled using GEM tools.~~

We describe the development of a new comprehensive PSHA model for North Africa using GEM tools. The source model combines active faults and distributed seismicity, the former constrained from published geological descriptions and geodetic data, while the latter from the harmonisation of published earthquake catalogues.

1 Introduction

The African continent is a mosaic of tectonically-stable Precambrian cratons, with the exception of the East African Rift System, the Cameroon Line, and the northern continental margin.

~~Unlike the most internal parts of the continent, characterized by the presence of large and stable cratons of Precambrian origin, the Northern margin of Africa is known to be tectonically active.~~ The complex interaction between the European and African plates, varying from transpression in the west to transtension and transform in the east, has caused substantial crustal deformation, often associated with the development of moderate on- and off-shore seismicity. Several damaging earthquakes, including some which have caused considerable economic loss and fatalities, have been reported within this wide seismic belt of more than 5000 km, extending discontinuously from Morocco to Egypt.

In recent times, the rapid development of North Africa countries, together with the progressive concentration of population in urban areas, has further increased the potential impact of large future earthquakes on the society (Benouar et al., 1996). The progressive enforcement of seismic norms and building codes has drawn attention to the need for a robust assessment of the seismic hazard. Therefore, with the goal of establishing common earthquake risk mitigation strategies, a state-of-art assessment of the seismic hazard of this region—homogenous across countries—is of paramount importance.

Several hazard studies have been carried in the past, either using probabilistic or deterministic approaches (e.g. El-Sayed et al., 1994; Benouar et al., 1996; Peláez et al., 2006; Ezzelarab et al., 2016; Mourabit et al., 2014, Lagesse et al., 2017). Nonetheless, most of these studies were conducted for specific target areas or at national scale, while very few attempts are documented for the evaluation of the seismic hazard at regional or either at continental level. The first important effort in this direction dates back to 1999 with the GSHAP project (Giardini, 1999) and very few advancements have been reported since then (e.g. Jiménez et al., 1999). Additionally, the lack of seismicity information available for some regions has strongly affected the quality and reliability of the corresponding hazard estimates, with an impact on the level of epistemic uncertainty.

In this paper, we describe a new probabilistic seismic hazard model developed for North Africa (herein also indicated with the NAF acronym) by the GEM secretariat, as part of the global mosaic of earthquake hazard model initiative (Pagani et al., submitted). The NAF model is based on the most up-to-date information from openly accessible datasets and scientific literature. The model is innovative in that it consists of a combination of mapped active faults, whose spatial pattern and activity rates have been derived from geological and geodetic observations, and distributed seismicity based on the direct analysis of regional and global earthquake catalogues. The combination of these two components aims to compensate for the relative limitations of the two sources of information, producing then a more robust estimate of the seismic hazard at regional scale, better accounting for the overall epistemic variability of the evaluated hazard.

2 Seismotectonic Settings of North Africa

2.1 North-West Africa (Ibero-Maghreb domain)

The geodynamics of North-West Africa is primarily controlled by the interaction between the Nubian and Eurasian plates (e.g. Patriat et al., 1982). From west to east, relative motion along such plate boundary is highly variable (Cherkaoui & El Hassani, 2012), ranging from the divergence of the Central Atlantic ridge system, pure strike-slip with dextral displacement of the Azores (e.g. Gloria fault), to a more complex

compressional regime along the continental margin between Iberia and Morocco (Gibraltar region), with oblique convergence with respect to the plate boundary (Peláez et al., 2007). This last tectonic setting is largely responsible for the continental seismicity of North Africa, with development of large thrust systems and orogenic belts (Atlas and Betic/Rif chains). The convergence rate in this region is rather variable, with values ranging from 3 to 6mm/yr (e.g. Argus et al., 1989; De Mets et al., 1990).

2.1.1 Morocco

Seismicity of Morocco is moderate, although destructive earthquakes are reported from historical and instrumental catalogues, such as the Agadir (Mw 5.9) and Al Hoceima (Mw 6.3) events, which caused about 12,000 and 629 fatalities respectively (Cherkaoui & El Hassani, 2012).

On-shore seismicity can be grouped in at least two main seismic provinces of the Atlas and the Rif structural domains. The Atlas chain extends from Agadir, as the High Atlas, to the northeast and is in continuation with the Saharan Atlas orogenic belt. Two adjacent but formally separated sub-provinces, namely the Middle Atlas and the Anti-Atlas, can also be identified by moderate seismicity and by a complex system of reverse and potentially active faults. The Rif structural domain is an orogenic system (the Maghrebides) that extends to Iberian Peninsula through the Strait of Gibraltar as the Betic Cordilleras, encompassing the extension-related Alborian Sea and the Algerian basin (Peláez et al., 2007). The Rif extends to the east into the seismic province of the Algerian Tell Atlas.

Off-shore seismicity is predominantly located in the Atlantic along the Azores-Gibraltar shear belt and within the Mediterranean basin in the Alboran Sea. The two domains are characterised by different geodynamic evolution of the underlying lithosphere, as evidenced by the distribution of earthquake source mechanisms. While the former domain shows mostly large and well-localised strike-slip events, the latter exhibits more diffuse seismicity (Jiménez-Munt et al., 2001) with extensional (normal) and generally smaller magnitude earthquakes (Cherkaoui & El Hassani, 2012).

Hypocentral depths are in most cases quite shallow (<30 km), although several events have been generated at intermediate (>30 km) to large depth (>60 km), particularly on the reverse faults of the High Atlas and the Rif/Western-Alboran province (Peláez et al., 2007; Medina et al., 2011).

2.1.2 Algeria

Algeria shows considerable seismicity, particularly in the northern part of the country, mostly related to the orogenic compressional domains of the Tell Atlas and (to a minor extent) the Sahara Atlas (Benouar and Laradi, 1996). The Tell is the continuation of the Moroccan Rif, and it originated within a similar tectonic regime. Local systems of folds and thrusts with roughly NE-SW alignment (Bouhadad and Laouami, 2002; Hamdache et al., 2010b) are responsible for the development of several important clusters of seismicity (Meghraoui, 1988; Hamdache et al., 2012). In contrast, seismicity of the Saharan Atlas is lower and less localized, with few moderate earthquakes. The two chains are separated by a relatively aseismic region of elevated topography (the High Plateaux) assumed tectonically stable, as no significant Meso-Cenozoic deformation is evident (Peláez et al., 2003). Moving to the east along the coastline, at the border with Tunisia, seismicity decreases.

The largest and most destructive earthquake recorded in recent time was the 1980 El Asnam event (Mw 7.1, Ms 7.3; Ouyed et al., 1983), although many damaging events with magnitude larger than 5.5 have been reported along the Tell Atlas (Benouar, 1994; CRAAG, 1994). Several epicentres have been localized in the vicinity of Quaternary basins (e.g. Meghraoui 1986; Hamdache et al., 2010b), whose geometric configuration and unconsolidated young sediments increase the possibility for site-specific amplification effects on the ground motion. Moreover, the earthquake risk is here exacerbated by the combination of high population density, building typology and high seismicity along the coastal region (Benouar, 1993).

2.1.3 Tunisia

Tunisia is located at the eastern edge of the Atlas chain, where the two main tectonic provinces of the Tell and Saharan Atlas gradually approach each other before intersecting the Zaghouan fault system, which is the most significant tectonic feature of the region (Ambraseys, 1962) crossing the country roughly NE-SW. Seismicity is mostly localized in the central and north part of the country (Ksentini & Romdhane, 2014), on a number of structures accommodating a sequence of contractional (folds and thrusts) and extensional (normal back-arc) regimes, often through the development of

left-lateral strike-slip mechanisms (Ben Ayed, 1993; Bouaziz et al., 2002). Late Quaternary seismic activity in Tunisia is overall moderate, but locally intense (Mejri et al., 2010). Although instrumental seismicity does not exceed magnitude 6 (Ksentini & Romdhane, 2014), a few large damaging earthquakes have been reported in historical times, such as the 408 AD event in Utique and the 856 AD event in Tunis (Vogt, 1993).

2.2   North-East Africa

In contrast to North-Western Africa, the geodynamics of the North-Eastern region is controlled by the relative movements of three plates: Nubian, Eurasian and Arabic. While Nubian and Eurasian have relative convergent motion, Africa moves progressively away from the Arabic peninsula, due to incipient spreading of the Red Sea oceanic ridge. The sinistral relative motion of the two margins is then accommodated by the presence of a transform region, the Dead Sea fault system, where the largest earthquakes have been historically recorded.

2.2.1 Egypt

Seismicity of Egypt is low to moderate compared to North-Western Africa and even more so compared to the high-seismicity of the neighbouring Hellenic and Cyprus subduction arcs and the Dead Sea transform region. Nonetheless, local moderate earthquakes pose a major threat to the population (Sawires et al., 2015), as evidence by the 1992 Cairo event (mb 5.8, Ms 5.9), which caused 561 fatalities, and by the historical 1847 event (Ms 5.8; Ambraseys et al., 1994). Furthermore, several highly populated areas are located on top of the fertile Nile alluvium (e.g. Said, 1981), whose low seismic velocities have large potential for site-amplification effects (e.g. Adly et al., 2017), greatly increasing the local earthquake risk (Badawy et al., 2016).

In relation to the transtensional stress regime caused by the spreading Red Sea margin, the large majority of earthquakes are characterised by normal faulting with variable strike-slip components, which increases toward the edge of the Sinai sub-plate. Only a minority of events have reverse focal mechanisms, mostly inland (Badawy, 2005).

2.2.2 Libya

The instrumental earthquake record of Libya is limited, due to the lack of appropriate seismological networks in the country till recent times (Hassen, 1983), with the establishment of the Libyan National Seismological Network (LNSNS). Regional seismicity is presently considered moderate to low. Nonetheless, large historical earthquakes are reported in literature (Campbell, 1968), such as the 1183 event, responsible for the destruction of Tripoli and that caused more than 20,000 fatalities (Kebeasy, 1980) and the more recent Ml 7.1 earthquake (1935), in the area of NW-SE trending Hun Graben (Suleiman et al., 2004).

With the exception of few known and potentially seismogenic geological structures in the North-West (e.g. the Hun Graben), the overall inland seismicity appears rather diffuse, as typical of stable continental tectonic conditions (Al-Heety & Eshwejdi, 2006). However, the offshore has a non-negligible activity, tectonically controlled by the presence of the nearby Calabrian and Hellenic subduction zones (Lagesse et al., 2017).

3 Methodology

In this study, the seismic hazard of the North Africa is evaluated probabilistically (e.g. Cornell, 1968, McGuire 2004) following the methodological formalism of Field et al. (2003) as implemented in the OpenQuake engine (Pagani et al., 2014), an open source seismic hazard and risk calculation software developed, maintained and distributed by the Global Earthquake Model (GEM) Foundation.

The proposed seismic source model consists of a combination of distributed seismicity and finite faults, the former calibrated on occurrence analysis of publicly available earthquake information, while the latter was derived from a thorough evaluation of information from both geological literature and direct analysis of GPS velocity fields.

In the following we describe in detail the different components of the North African hazard model, including the creation of a homogenised earthquake catalogue for the region, the active fault database and the seismicity analysis (occurrence model, source mechanism distribution, spatial pattern of hypocentres). Separate sections are then

dedicated to the regional selection of most suitable ground motion prediction models and to the treatment of the epistemic uncertainties using a logic-tree approach.

4 Compilation of a Homogenised Earthquake Catalogue

The availability of a complete (in space and time) earthquake catalogue with homogeneous magnitude representation is an unavoidable requirement for the proper definition of the past (and forecasting of future) earthquake occurrences in probabilistic seismic hazard assessment. Although several attempts to create an earthquake catalogue exist for the region (e.g. Peláez et al., 2007; Medina, 2010; Hamdache et al., 2010a), many of these catalogues were compiled for relatively small areas, generally within national projects, and lack a proper magnitude homogenisation. For the purpose of having a unique catalogue valid for the whole North Africa, we created a new Mw-homogenised earthquake catalogue by assembling globally and locally available sources. The GEM implementation of the North Africa Earthquake Catalogue (hereinafter GEM-NAEC, Figure 1), presently consists of 5170 events with $4 \leq Mw \leq 8.5$, covering a period from 1016 to 2013. The general philosophy adopted for the construction of this catalogue resembles the one adopted by Weatherill et al. (2016); in the following we describes the various steps completed for the construction of this dataset.

4.1 Source Information

For the creation of the GEM-NAEC we collected an extensive set of catalogues (see Table 1), which includes:

- ISC-GEM catalogue (Storchak et al., 2013; 2015; Di Giacomo et al., 2018); we assume this to be the most reliable and complete compilation, but is limited in its time span (> 1900) and minimum magnitude (> M_W 5.5);
- ISC-REV, the manually reviewed bulletin from the International Seismological Centre (ISC 2013) (Storchak et al. 2017; www.isc.ac.uk);
- GCMT/Harvard Bulletin (Ekström et al., 2012);
- IGN catalogue (compiled by the Instituto Geográfico Nacional, www.ign.es);

- EMEC catalogue (Grünthal & Wahlström, 2012);
- GEM Global Historical Earthquake Catalogue (GEM-GHEC, Albini et al., 2014).

4.2   Hypocentral Location Selection

An important mandate of the International Seismological Centre (ISC) is to collect earthquake information from ~~several~~ seismological organisations worldwide. In most cases, however, different magnitude and location (including origin time) solutions are available from the different reporting agencies for a specific event. Hence ISC also provides its own solutions, relying on picked phases and waveforms directly provided by local and global networks. When multiple hypocentral locations are then available, ISC flags its preferred choice as "Prime", which is often—but not always—the ISC's own solutions. In this study, we assume the Prime solutions are always the most reliable within the ISC compilation (Table 2).

Prioritisation of location solutions when comparing other catalogues, however, requires more attention. As a rule, we consider the hypocentre locations from the ISC-GEM catalogue as best estimates, due to the accurate review process undergone. Unfortunately, a rather limited number of events are available in North Africa from that compilation (see Table 1). The GCMT bulletin uses in most cases ISC solutions and therefore no selection is usually required, with the exception of very few events. Similarly, IGN is a reporting agency of ISC (with code MDD), however, not always considered as Prime. We use then the IGN solutions only for the subset of events not included or not yet reviewed by ISC (e.g. after 2014). Finally, EMEC and GEM-GHEC are mostly used to complement historical seismicity information. Given the rather uncertain hypocentre locations of historical events, we assigned it the lowest priority in the ranking.

4.3   Duplicate Finding and Catalogue Merging

Once assigned a priority rank to the solutions, a non-trivial task is the identification of duplicated events between catalogues. In this study, the search is done using a duplicate finding algorithm based on spatial and temporal matching of the solutions within pre-defined windows, whose length is tuned according to the expected accuracy

of the solution in a specific time period. ~~In~~ Table 3 summarizes the length of the time (Δt) and space (Δd) windows used for the three main periods of analysis. As it can be seen, the window size decreases from historical to more recent times. It must be noted that month/day information is available for the large majority of the analysed historical records and only a restricted number of uncertain events required manual review. For these events is was assigned an arbitrary occurrence date of January 1st.

It is worth mentioning that, being an automated process, misidentification errors are possible. As a matter of fact, no unique window length exists that allows capturing all duplicated events between catalogues, without erroneously including a fraction of independent events. Window size is then manually adjusted to obtain best trade-off between the two edge cases. Fortunately, in most cases erroneous duplications are found between events of an aftershock sequence, which are nonetheless removed afterwards when declustering is applied.

Once duplications between catalogues have been identified, merging is then performed. Corresponding duplicated events are collapsed into a single event with multiple solution representation, while unique events are simply added. As a final step, the preferred solutions are selected according to the previously defined priority rules. The result of this selection is presented in Table 4.

4.4   Magnitude Homogenisation

A key point in the homogenisation process is representing all available earthquake events using a unique target magnitude. In this study, we use as a reference type the moment magnitude M_W (Hanks and Kanamori, 1979), due to its ~~direct~~ relation to released energy and the lack of a saturation effect. Unfortunately, M_W has only been systematically reported by global agencies in relatively recent times (e.g. after 1976 for the GMCT catalogue). Moreover, although M_W is nowadays widely accepted as the most suitable representation of earthquake size, many agencies are still reporting in other formats, sometime for backward compatibility or simply for lack of expertise.

Magnitude conversion is nonetheless not a straightforward process (e.g. Weatherill et al., 2016), often affected by large uncertainties and biased by the effect of magnitude saturation, inconsistent processing algorithms and/or intrinsic regional variability. Moreover, the quality of the reported magnitude is highly variable between agencies, mostly due to network limitations (e.g. number of stations, distance, azimuthal

coverage). ~~For all these reasons, we apply in this study a magnitude homogenisation approach that is two-steps; first through an extensive data selection and by subsequently performing magnitude conversion.~~ For all these reasons, we used a two-step approach to homogenization, carefully evaluating the earthquake catalogues prior to magnitude conversion.

4.4.1 Agency and Magnitude Type Selection

In the first step, we explore the availability of different magnitude types from each available reporting agency. A ranking scheme is created based on defining priority rules, similarly to what was done for location solution selection. In general, prioritisation is made based first on a magnitude type classification (from higher to lower reliability: Mw → Ms → mb → Ml → Md) and then following agency-specific selection criteria. The proposed priority rules are summarized in Table 5.

By applying these rules, a single "best" magnitude estimate is then selected for each event with multiple magnitude representation (either natively reported from ISC or after catalogue merging).

4.4.2 Magnitude Conversion

When converting between magnitude scales, best practice would be to locally calibrate ad-hoc conversion rules for each reporting agency and magnitude type against the reference scale (in this case, M_W). However, the amount of records available for North Africa was not sufficient to perform ad-hoc calibrations, with the exception of very few agencies, such as Ms and mb magnitudes from ISC and NEIC. For these cases, however, the African subset is in close agreement with globally calibrated models, such as those in Weatherill et al. (2016) or Di Giacomo et al. (2015). For other agencies and magnitude types with too few reported events, some grouping was necessary to perform a reasonable statistical analysis. We therefore decided to rely only on globally calibrated relations (see Table 6). It has to be noted that duration magnitude is usually calibrated on a separate dummy magnitude type, which is variable between the different reporting agencies. Due to the aforementioned lack of magnitude calibration pairs and the significant data scatter, it appeared more appropriate to just apply a simple 1:1 transformation, assigning nonetheless an arbitrary high uncertainty to the conversion.

5 The active fault database

In order to provide sources for fault-based PSHA, a new dataset of active faults in North Africa was created, containing ~125 active fault traces (see Figure 2). Faults were mapped on topographic data (typically 30m SRTM) based on mapping in the literature as well as interpretation of topographic, seismic and geodetic data. A small amount of metadata, including attributes for each fault trace describing the geometry, kinematics, slip rate, and epistemic uncertainties were collected for each fault if present in the literature, or estimated from the raw data otherwise. The faults are publicly available at https://github.com/GEMScienceTools/n_africa_active_faults (last access 20th September 2019) in a variety of GIS formats. Fault sources for hazard modelling were made from this data, with a few small or geometrically uncertain faults removed, and slip rates estimated for all structures even if no published rates were available. Slip rate estimates were made through expert judgement of the geodetic and seismic data, as well as consideration of geomorphic expression and similar, better studied faults in the region.

Of the ~125 active structures, about half were based directly on published work, typically field studies by local scientists. Fault characterization based on topographic, geophysical and geodetic data was only performed when no studies for that structure were available. The majority of faults that are not based on published studies are along strike or otherwise close by the faults that have received direct investigation, and clearly share some characteristics of the studied faults. The reference information for each fault is given in the fault database.

We acknowledge that involvement of local scientists in the creation and maintenance of the fault database is ideal; unfortunately, we were not able to establish these collaborations within the time constraints of this project. However, we stress that the NAF seismic hazard model presented here is simply the first version, and that local scientists who wish to be involved in future iterations are strongly encouraged to contact the GEM Secretariat (hazard@globalquakemodel.org).

5.1   High and Middle Atlas

The major seismogenic features in the High and Middle Atlas are range-bounding reverse faults that dip towards the interior of the mountains. Active faulting seems restricted to the range fronts (e.g. Sébrier et al., 2006). Many of the faults were formed during Mesozoic extension, and were later reactivated as reverse faults, and therefore retain the steeper dips than primary reverse (thrust) faults (e.g. Peréz et al., 2019).

The western High Atlas are bound by the North and South Atlas Faults, on their respective sides of the range. These are 250-500 km long, moderately-dipping reverse fault zones, capable of large earthquakes. The North Atlas Fault appears continuous at the surface along much of its length, though the South Atlas Fault is clearly segmented. The shortest, westernmost segment was likely responsible for the 1960 Ms 5.9 Agadir earthquake (Meghraoui et al., 1999), which killed ~15,000 people (Paradise, 2005). Slip rates on these faults are estimated at 0.1-0.5 mm/yr (e.g. Meghraoui et al., 1999; Sébrier et al., 2006).

Farther east, the High Atlas is bound on the north by the Beni-Mallal Fault, which is quite similar to the North Atlas Fault (Arboleya et al., 2004). The southeastern High Atlas, faulting on the southern side is expressed in discontinuous thrusts in the northern Ouarzazate Basin; Pastor Castilla et al. (2013) have estimated shortening rates here of 0.1 mm/yr. Reverse faulting is more distributed in the Middle Atlas. Reverse-sinistral faults are present in the Middle Atlas and the Midelt Basin between it and the High Atlas; those that have been studied yield slip rates around 0.05-0.5 mm/yr (e.g. Gomez et al., 1996; Rigby, 2008).

Though seismicity is present in the Saharan Atlas, it is largely strike-slip on either NE- or NW-striking fault planes. No similar structures are evident in the topography, suggesting that these earthquakes occur on immature faults that have not yet propagated to the surface and caused significant displacement.

5.2   Rif

The Rif Cordillera in northern Morocco is a complicated segment of the African-European plate boundary. The zone is arcuate, with sinistral-reverse faults in the south and southwest, reverse faults in the west, and normal faults in the east accommodating the transition to the Tell Atlas. The faults are long and fairly straight, and segmentation is unclear; our interpretation of the topography and literature suggests segment lengths of ~150 km. Geodetic and geologic evidence suggests that these faults slip ~1 mm/yr.

5.3 Tell Atlas and offshore faults

The Tell Atlas stretch along the North African coast from the Morocco-Algeria border through northern Tunisia. Deformation is transpressional (reverse and dextral) along ~ENE-striking faults (e.g. Meghraoui and Pondrelli, 2013). In the western half, most active faults onshore are reverse or reverse-dextral faults in a valley between the coast and the high interior of the range. These faults have slip rates ~1 mm/yr (e.g. Meghraoui et al., 1988; Maouche et al., 2011) and have produced a number of upper crustal earthquakes of up to M 7.1 in the past century (e.g. Kariche et al., 2017); some of these have been extremely damaging, particularly the 1980 Mw 7.1 event on the El Asnam fault, which killed several thousand people (Ambraseys, 1981) and caused damages of 22% of Algeria's GDP (GEM-ECD).

Another set of reverse and reverse-dextral faults exists north of the Maghreb coastline. These faults break the submarine crustal surface about 20 km offshore, and dip southward at shallow angles (e.g. Mauffret, 2007). These faults are largely known through marine geophysical imaging, and little information exists as to their slip rates or lateral continuity. Nonetheless, they probably accommodate at least half of the ~5 mm/yr of convergence between Europe and Africa at this longitude (e.g. Serpelloni et al., 2007).

5.4 Tunisia

Within the Aurès Mountains of Tunisia and easternmost Algeria, faulting is less organized. Normal faulting on NW-striking planes is present in the center of the Aurès creating several prominent grabens; dextral faulting is also found in the region (Said et al., 2011). The eastern margin of this zone shows sinistral-reverse slip on the N-S Axial Fault (Soumaya et al., 2015). To the north, at the eastern terminus of the Tell Atlas, seismicity is distributed throughout but the geomorphology is complicated by previous deformational episodes, and no clear Quaternary faults can be distinguished.

The southeastern margin of the Atlas in eastern Algeria and western Tunisia is characterized by thrusting on large, distributed and very shallowly dipping faults. Shortening rates on the measured structures are ~0.1 mm/yr (Saïd et al., 2011), and the

unmeasured structures nearby have similar geomorphic and structural expression, suggesting similar deformation rates.

5.5 North-Eastern Africa

Deformation in northeastern Africa is largely extensional, relating to intraplate stresses and the transtensional motion of the Arabian plate with respect to Africa rather than Africa-Europe dynamics. Although both normal fault and strike-slip focal mechanisms are present throughout northern Libya, the only mappable faults with confirmed Quaternary activity are the normal faults making up the Hun Graben (e.g., Abdunaser and McCaffrey, 2015).

Northeastern Egypt is very active seismically, relating to the ongoing extension across the Red Sea and the Gulf of Suez. Most faults on both the African and Sinai margins of the Gulf of Suez are normal fault striking NNW, parallel to the Gulf (e.g., Sharp et al., 2000). Those closest to the Gulf accommodate much of the extension between Sinai and Africa (e.g. Bosworth and Taviani, 1996), with slip rates of 0.5-1 mm/yr, based on the ~2 mm/yr GPS velocity gradient (Mahmoud et al., 2005). The northeastern Egyptian coast also has faults striking perpendicular and obliquely to the main structural trend. The most prominent faults are those bounding Wadi Araba and the Galala Plateau. Though they are not previously mapped as such, the topography and satellite imagery strongly suggest that Wadi Araba is an active graben, albeit with a very low extension rate (~0.1 mm/yr), and potentially only a few hundred meters of offset.

Despite damaging earthquakes near Cairo (Hussein et al., 2013), no surface faults in the Dahshour Seismic Zone or the surrounding region could be identified in the topographic or satellite imagery that may be related to these events, or display other indication of Quaternary activity; therefore, regional earthquakes may be of only small to moderate size. The 1981 Aswan earthquake likely ruptured a section of the Kalabsha Fault (Mekkawi et al., 2005), and is thought to have been triggered by the impoundment and filling of the Aswan Reservoir.

6 Seismic Source Characterisation

The North Africa earthquake source model consists of a combination of distributed seismicity and finite faults, the former based on the analysis of the previously obtained homogenized earthquake catalogue, while the latter based on the available slip rate information from geologic and geodetic observations. The goal is to compensate for the reciprocal limitations of the two datasets, on one hand to better constrain the long-return periods of the known major tectonic structures and to complementarily account for spatial variability of the earthquake process.

In the following section, the main characteristics of the two source typologies are discussed.

6.1 Distributed Seismicity

6.1.1 Source Zonation

The study area has been initially discretized into 54 independent source zones, following the guidelines proposed by Villanova et al. (2014) that provide a set of objective criteria to delineate regions of supposedly homogenous seismic potential. The main constraint for the development of the source model came from the analysis of the earthquake catalogue (stationarity of the completeness periods, evaluation of the mean activity rate, distribution of seismogenic depths) and from a set of geological and seismotectonic considerations, such as style, geometry and distribution of existing faulting systems and their relation to the local stress and deformation regimes (see discussion in section 6.2.2). Local and regional source models from previous hazard studies (e.g. Ezzelarab et al., 2016; Lagesse et al., 2017, Peláez et al., 2018) have also been taken into great consideration as starting point for the proposed zonation and to ensure compatibility across the borders, particularly with the SHARE (Woessner et al., 2015) and EMME (Giardini et al., 2016; Danciu et al., 2017) models.

The 54 source zones have then been gathered into nine main tectonic domains (Figure 3), assumed to have comparable rheological and mechanical behaviour with respect to the underlying crustal geology under the regional stress regime. Source grouping is particularly useful for earthquake occurrence analysis in low seismicity regions (Poggi et al., 2017), where the limited earthquake record might be insufficient for the proper calibration of poorly constrained seismicity parameters, such as the maximum magnitude or the slope (b-value) in cases where a negative-exponential

frequency-magnitude model is used (see following section for further details). As well, tectonic grouping has also been used for the regional characterization of main faulting style and hypocentral depth distribution of the seismic source model.

6.1.2 Occurrence Model and Maximum Magnitude

Earthquake occurrence of the distributed sources is modelled using a double-truncated Gutenberg-Richter (GR) relation. The fit of the GR relation is done for each zone on the observed annual rates obtained after completeness analysis of the declustered earthquake catalogue, following the approach described in Poggi et al. (2017), which we refer for a more comprehensive description of the methodology. The minimum magnitude used for calibration is variable between zones, depending on the completeness of the local earthquake record. For the hazard calculations, however, a common magnitude threshold of 4.5 has been arbitrarily assigned to all zones, assumed as the lowest magnitude considered capable of generating sensible damage.

Maximum magnitude (M^{max}) is also variable between source zones and is generally derived as the size of the largest observed (M^{obs}) event plus 0.5 magnitude units. This increment is assumed as a sufficiently conservative choice for the region, although further uncertainty is nonetheless accounted for in the source model logic tree (see Section 9). It must be noted, however, that the definition of such parameter is not critical for the calculation at 10% probability of exceedance (475 years return period), which is mostly controlled by the intermediate magnitude range, but might require some further investigation if longer return periods are to be considered.

The fit of the GR relation is done in each zone on the observed annual rates obtained after completeness analysis of the declustered earthquake catalogue. The fit of the GR is performed in two separate steps and by mean of a non-linear least square approach on non-cumulative rates (Poggi et al., 2017). Such technique proved to be useful in case of limited earthquake records by the introduction of uneven magnitude bin widths, typically of increasing size from small to large magnitudes. The bin size is defined while performing completeness analysis and is progressively adjusted after several iterations to provide an optimal solution of the GR. In general, the size is set be increasing with magnitude (e.g. 0.25 magnitude units from 4.5 to 5.25, then 0,5 above 5.5), but in case of too few events (e.g. group 5), grouping is necessary. The process requires nonetheless a level of personal interpretation based on expert judgement.

In a first step, a preliminary occurrence model is obtained for each seismotectonic group (Figure 4), using the largest M^{max} (=M^{obs}+0.5) of all zones within the group. From that, regional b-values are derived. In a following step, activity rates (a-values) are obtained for the single zones while imposing the previously established regional b-value from the corresponding group. This approach was necessary to obtain more stable results in those areas of the study region with rather short or incomplete earthquake records. A summary of the derived seismicity parameters is given in Table 7.

6.2 Spatial Variability of Earthquake Occurrences

To better represent the spatial variability of seismicity across the study area, the annual occurrence rates previously obtained for the homogenous source zones have been redistributed within each polygon using a procedure that accounts for the irregular spatial pattern of the observed events. The procedure shares some similarity with the popular smoothed seismicity approach (e.g. Frankel, 1995), but is more convenient in that a unique fit of the magnitude-frequency distribution is here required for each zone. The total earthquake occurrence is redistributed within the surface of the corresponding polygon taking into account the spatial density of earthquakes by means of a seismicity smoothing kernel. Moreover, the combined use of zones gives the possibility to account for different modelling parameters (b-value, depth distribution, rupture mechanism) in separate neighbouring regions.

The procedure is described as follow. In a first stage, each source zone is discretized into a grid of point sources. A spacing of 0.1 degrees (about 11 km) is used, which provides a rather dense sampling of the area but at the same time is not computationally demanding. For each discrete location i, then, the occurrence rate is assigned a fraction of the total annual rate (R) for the zone, scaled by a normalized weighting function (W) that accounts for the relative distance to all neighbouring events j:

$$R_i = \frac{W_i}{\sum_{k=1}^{Ntot} W_k} R \qquad\qquad \textbf{Eq. 1}$$

where *Ntot* is the total number of points in which the area has been discretized. In such way, more seismically active regions of a source zone are modelled using point sources of proportionally higher productivity. It is important to notice that, due to the

18

normalisation, the overall rate balance for each zone is nonetheless preserved when summing the activity rates from all the discrete point sources.

The weighting function is calculated from all the events (*Etot*) within the zone (plus a small buffer of about 0.1 degree to minimize edge artefacts) as:

$$W_i = \sum_{j=1}^{Etot} e^{-0.5\left(\frac{D_j}{\lambda}\right)^2} \qquad \textbf{Eq. 2}$$

where D is the epicentral distance and λ is a distance decay parameter controlling the influence of far events and therefore influencing the "smoothing" of the rates across the area (e.g. Figure 5). A theoretical infinite value of λ would produce a homogenous area source.

Unfortunately, the choice of an optimal decay parameter λ is still under investigation and currently rather subjective. Although we found that a value of 50 provides a more realistic seismicity pattern for the seismogenic model of the study area (Figure 6), the proposed value might not generalize to other regions, for example with lower activity and significantly incomplete catalogues. To account for the epistemic ambiguity of this parameter, however, three different values of 25, 50 and 100 are used with variable weight in a logic tree approach (see Section 9).

6.2.1 *Hypocentral Depth Distribution*

By analysing the available depth solutions from the catalogue, it was possible to characterize the expected hypocentral depth distribution of the nine source groups separately. Each distribution consists of five depth classes, ranging from 0 to 50 km (Figure 7). For each class, the normalized density is calculated as the number of the events falling in that range, divided by the total number of events. This value is then assigned to the source model as the probability of the median depth of the class. It must be noted that the catalogue has been purged beforehand of any fixed depth solution (e.g. at 0, 10 and 33km), which would have biased the statistic.

Overall, the observed seismicity regime reflects the transition between a stable continental crust, characterised by low attenuation and relatively deep earthquake hypocentres, to typical active shallow crust. In the study region, although seismicity is

predominantly localized within the first 20-25km for most of groups, in few cases a non-negligible fraction of the events extends to larger depths, as particularly evident for group 9.

6.2.2   Source Mechanism Distribution

Defining the dominant rupture mechanisms is an important part of the source model construction. This is necessary information when using ground motion attenuation relationships to compute the distance from the source to the site, which depends on the rupture geometry and distance metric used (e.g. Rjb, Rrup among other metrics, as described in Douglas, 2003). Such assessment is preferentially done by statistical analysis of the available fault-plane solutions from moment tensor inversion, but other constraints—such as the regional stress regime and local geological structures—can be integrated in case of lack of recordings or non-univocal rupture orientation.

We have analysed the available moment tensor solutions for the region from the GCMT catalogue. About 73 events were found, which were analysed using the program FMC (Álvarez-Gómez, 2014). The program produces a Kaverina et al. (1996) type classification diagram (e.g. Figure 8) as presented in Kagan (2005), where events are classified into seven main faulting styles, depending on the relative comparison of the B, P and T axis following the convention of Aki and Richards (1980). Unfortunately, the lack of events made impossible the use of such classification in some regions, where the decision on the dominant mechanism was then based on seismotectonic considerations. The result of the analysis for individual source groups is presented in Table 8, in the format required by the OpenQuake engine software.

7 Modelling of the fault sources

Nowadays it is common practice to model fault sources as three-dimensional (3D) surfaces, supplemented by additional information describing the style of faulting, the range of magnitudes generated and the frequencies at which events may occur. In the following, we describe the methodology we adopted to integrate the shallow fault component into the NAF model.

Each fault previously characterized in the North Africa active fault database is modelled as "Simple Fault", following the convention used for the OpenQuake engine. This type of fault source consists of a surface obtained by projection of the fault trace along the dominant (constant) dip. Although approximated, this approach provides an easy way to account for rather complex geometries, assuming nonetheless no significant variation of dip with depth, which makes it particularly suitable for shallow seismicity. The full list of parameters required for the definition of a fault source and the assumptions used to build the NAF model are given in Table 9.

At depth, each fault surface is bounded by the maximum seismogenic thickness, which is defined a-priori by seismotectonic considerations on the study region. The limit usually ranges between 10 – 25 km in an active shallow environment, but it could sensibly vary for oceanic (i.e. subduction interface) and intraplate strike-slip faults. It must be noted, however, that in case of very low dip angle the sole use of a maximum depth constraint might lead to unrealistic fault geometries. For this reason, additional depth constraints are included in the modelling following Leonard (2010, 2014).

During calculation, the OpenQuake engine discretizes the fault surface to a regular mesh, which represents the distribution of nucleation points of all possible ruptures along the fault. The spatial extent of each rupture is assigned based on the assumed magnitude scaling relation and rupture aspect ratio.

To model earthquake occurrences of faults, commonly used magnitude frequency distributions (MFD) are the aforementioned Gutenberg-Richter relation, the characteristic distribution (Schwartz and Coppersmith, 1984) and models based on a mixture of these (e.g. Youngs and Coppersmith, 1985).

For North Africa, we use a double-truncated Gutenberg-Richter distribution, in agreement with the occurrence model adopted for the distributed seismicity. Occurrences are then derived directly from slip rates, either measured or inferred by geodetic considerations, given the fault expression and geometry. The a-value for each fault is found by balancing the scalar seismic moment accumulation rate (the product of the fault's area, slip rate, a default shear modulus of 30 GPa, and the complement of an aseismicity coefficient described below) and the scalar moment release rate, from the integral of the incremental MFD. The b-value is imposed a-priori as derived from seismicity analysis as that of the source zone enveloping the fault. In case of faults falling between adjacent zones, the value is averaged proportionally to the extent of the fault trace within the different groups. The maximum magnitude of the MFD is derived

by applying the Leonard (2014) scaling relations, with the additional constraint of not exceeding the maximum magnitude ~~realistically~~ expected for the source group. An aseismic coefficient of 0.1 was used to account for the amount of accumulated seismic moment released aseismically by creep and plastic deformation. This parameter has a linear impact on the results, but is in fact loosely constrained, and trades off linearly with other parameters such as lower seismogenic depth or shear modulus. We envisage a more critical analysis of its sensitivity in a subsequent study.

From the original database, 115 fault sources have been modelled by an ad-hoc Python tool developed within the *Model Building Toolkit* of GEM. In fact, some faults were excluded being not capable of generating earthquakes larger than Mw 5.5 (lower magnitude-bound fixed).

The available modelled faults, however, cannot capture alone the whole seismic activity of the region. In order to use the fault source model as alternative to distribute source model (see Section 9), a complementary source background is therefore needed. The background was derived from the distributed seismicity model, by direct comparison of the earthquake rates between the two source models (faults and distributed seismicity) using the following procedure. In a first step, faults are discretized into arrays of point sources, with 1km spacing along the fault trace. Subsequently, the rates associated to each point are redistributed on the background reference grid using the same methodological approach used in Section 6.2 to assemble the distributed model. For consistency, the same kernel is used, in this case λ=50. Finally, the discrete rates derived from faults and from the distributed model are compared at each point of the mesh, and the rates in exceedance removed from the reference to construct the background.

8 Ground Motion Characterisation

The choice of an appropriate ground motion model is a critical step in definition of the hazard scenario. As for standard practice, if a locally-calibrated ground-motion model is not available, a set of most representative Ground Motion Prediction Equations (GMPEs) for a region should be selected through direct comparison against local earthquake recordings, in a range of magnitude and distance that are meaningful

for the analysis, or by the implementation of a backbone approach (e.g. Atkinson et al., 2014).

Unfortunately, the scarce availability of strong-motion recordings for the whole analysed North Africa belt makes a direct comparison impractical, or even impossible in some areas. Therefore, non-direct selection criteria have to be used instead, with special regard to matching of the tectonic context and suitability of the GMPE functional form (e.g. Cotton et al., 2006).

As for the case of a previous seismic hazard study for the East African Rift (Poggi et al., 2017), a combination of different seismotectonic conditions is expected for North Africa. While a low-attenuation stable continental crust (SCC) is to be expected in the most internal part of the continent, active shallow crust (ASC) conditions are likely at the more seismically active regions close to plate boundaries, such as the mountain chain of the Rif and Tell Atlas and regions surrounding the Red Sea. In this study, we rely on the global tectonic zonation proposed by Chen et al. (2018, Figure 9), which is based on Fuzzy Logic analysis of both seismological and geological information. Using this approach, North African source zones have been classified either as SCC (group A) or ASC (group B). An additional buffer region (group C) is also prescribed for transition zones of intermediate characteristics between SCC and ASC, in order to avoid abrupt variations of ground motion predicted by GMPE calibrated for different tectonic settings.

Following this classification, the same combination of ground motion prediction equations selected in Poggi et al. (2017) has been used, with respectively two models for ASC (Chiou and Youngs 2014; Akkar et al., 2014) and two models for SCC (Atkinson and Boore 2006; Pezeshk et al., 2011). The four ground motion models were selected because of their compatibility with the overall characteristics of the target region and based on the evaluation of the methodological robustness and the prediction performances from review of the existing literature. The selected GMPEs and their corresponding weights assigned to each tectonic group are summarized in Table 10.

9 Source Model Uncertainties

To account for epistemic variability of key model parameters, a source model logic-tree has been implemented. The logic-tree structure includes three cascading branching

levels, each one describing the assumed distribution of uncertainty of a specific and independent model parameter.

The first branching level addresses the uncertainty about the length of the smoothing kernel, whose definition is presently highly subjective. In this study we have selected three different smoothing distances (using a lambda parameter of 25, 50 and 100 km), used to produce three independent seismicity models. According to our judgement, the model computed using a length of 50 km is the most representative of the observed seismicity pattern. For that, a weight of 0.5 has been assigned. A slightly lower significance is then given to the two remaining edge models, each with a probability of 0.25.

The second and third branching levels are about the uncertainty on the maximum magnitude and the b-value, respectively. For the first parameter we have arbitrarily assigned a relative possible error of ±0.2, which we consider a reasonable epistemic variability for the +0.5 magnitude units used for the definition of the maximum magnitude (see section 6.1.2). For the b-value, we assigned an uncertainty of ±0.05, based on the observation of the GR fit variability when varying the size of magnitude classes of the occurrence model. In both cases, we assumed a weight of 0.5 for the central estimate and 0.25 for the edge values. A representation of the whole logic-tree structure is given in Figure 10, including the branching levels for both the source and the ground motion model uncertainties. Due to technical limitations, no uncertainty is presently considered for the fault model, but we plan to integrate also this variability in future developments of the NA model.

Although the full logic three has been used to explore the epistemic variability of the model, a simplified version has also been produced, with the goal of decreasing the calculation load, while preserving the mean hazard unmodified. This has been achieved by previous collapsing of the three distributed seismicity models into a single weighted average rate model, keeping weights as in the full logic-tree. Such model is presently integrated in the global mosaic of hazard models of GEM (Pagani et al., submitted).

10   PSHA Results

10.1 Calculation settings

Calculations were performed on a mesh of 87551 sites (on a hexagonal grid with approximately 10 km spacing) and for free-rock reference soil conditions with a shear wave velocity in the upper 30 meters (Vs30) of 800 m/s, corresponding to class A according to Eurocode8 (CEN 2004) and NEHRP (BSSC 2003) classification.

At each site, we compute ground motion probabilities of exceedance (PoEs) for 5% damped response spectral acceleration (in g) and investigation time of 50 years. The main target of this study is the 10% PoEs (corresponding to a 475 year return period, assuming a time-independent Poissonian model) as prescribed by the large majority of building codes, although 2% was also analysed to test the stability of longer return periods. Hazard curves (HC) were computed at PGA, 0.1 s, 0.2 s, 0.5 s, 1 s and 2 s, in relation to the periods allowed by the selected ground motion prediction models. A conservative 3 sigma truncation level was imposed to bound ground motion uncertainty integration. All calculations for this study were performed using Version 3.4 of the OpenQuake engine, which can be accessed at https://github.com/gem/oq-engine/tree/engine-3.4 (last access 25/06/2019).

10.2 Calculation results

The main output of the calculation are the hazard curves at each site and different spectral periods. From those, hazard maps and Uniform Hazard Spectra (UHS) are then subsequently derived. In the following, hazard curves and UHS are presented for four target North African capitals, considered of uppermost significance from a risk perspective: Algier (Algeria), Rabat (Morocco), Tunis (Tunisia) and Cairo (Egypt). Hazard maps, however, are presented for the whole calculation grid, as a means to compare regions of different hazard levels.

10.2.1 Earthquake hazard curves

We compute hazard curves for 25 logarithmically spaced bins of acceleration, ranging from 0.005 g to 4 g, and independently for all spectral periods from PGA to 2 s (Figure 11). It must be noted that PoEs falling between intermediate acceleration bins are extrapolated using log-linear interpolation, which is a fairly acceptable approximation for a sufficiently dense initial sampling.

Looking at the results for the four target sites, the shape of the hazard curves is rather stable between different spectral response periods, with the only noticeable exception of Rabat, which shows a visible kink of the PGA curve at around 0.1 g. This is likely due to combined effect of faults and distributed sources, which are controlling different probability levels of the model. Such effect becomes evident because of the relatively lower seismicity of the region, when compared to the other capitals.

10.2.2 Uniform hazard spectra

Uniform Hazard Spectra (UHS) were computed for 10% probability of exceedance in 50 years for the four North African capitals. As visible in Figure 12 and as it is also generally expected (e.g. Poggi et al., 2018), the larger amplifications are experienced at intermediate periods, roughly between 0.1 s and 0.2 s. In these plots we also compare the mean UHS with 0.15, 0.5 and 0.85 quantile curves, to give a first order representation of the epistemic variability associated with the model. It is interesting to notice the mismatching between mean curve and the 0.5 quantile, particularly evident for Algiers and Cairo, where the hazard is higher. Here, while the mean is generally shifted toward slightly larger accelerations, it is also evident an overall asymmetry of the uncertainty distribution, which is due to the presence of cluster of models from different log-tree end branches. Due to this evident asymmetry, the 0.5 quantile might be a more suitable representation of the intermediate hazard level.

10.2.3 Earthquake hazard maps

Hazard maps were computed at PGA for 10% probability in 50 years (Figure 13). Other spectral periods have also been considered for evaluation, but are not discussed here, as they would not bring additional information.

Overall, the computed hazard pattern clearly reflects the distribution of the observed seismic events from the catalogue and the location of known active faults. As expected, the largest accelerations are located at the northern margin of the Maghreb countries, mostly along the Rif and Tell Atlas chains. By comparing the results from the composite model (Figure 13a) and just from faults (Figure 13b), it is evident that hazard is here mostly controlled by the modelled active structures, while toward south (Saharan Atlas) the contribution of fault sources is less evident. A minor but definitely

not negligible acceleration level is then evident in North-Eastern Egypt, as it was also seen from the analysis of UHS (Figure 12). More difficult is to evaluate the reliability of the hazard in Libya, where the lack of data and seismotectonic information is critical. Potentially debateable are also the two isolated spots near Assuan (Egypt) and at the border between Mauritania and Western-Sahara, which could also be linked to the occurrence of triggered seismic events.

11 Discussion and Conclusions

We described a new probabilistic seismic hazard model for North Africa, based on publicly available and newly collected information for the region. The earthquake occurrence model developed combines active faults with earthquake sources defined using the earthquake record available for the region. Despite the challenges of identifying and characterising faults in this region, the produced model provides a more complete characterisation of earthquake occurrence compared to hazard models created using primarily past seismicity. We are conscious that our model certainly suffers from the lack of calibration of data in certain areas such as in Libya, where the historical (macroseismic) and instrumental earthquake record we collected is certainly incomplete. Moreover, our model does not fully describe the variability of occurrence rates over depth, as a unique one-dimensional depth distribution is still used within each source group. In a future improvement, therefore, we plan to extend the rate-redistribution algorithm to account also for depth dependency, in order to simulate a fully three-dimensional distributed source model

When compared to the results from the GSHAP project, our model provides a more comprehensive representation of the spatial variability of hazard, due to the integration of both faults and observed seismicity to constrain the spatial geometry and temporal occurrence of the modelled distributed sources.

As for the case of the sub-Saharan hazard model previously developed by the GEM Secretariat, one of the major issues is the lack of publicly accessible strong ground motion recordings for the implementation of reliable regionally-calibrated ground motion prediction models, or alternatively for the validation of existing ones. This issue is critical, as it is nowadays evident that GMPE selection has a large impact on the computed hazard. Nonetheless, the situation is likely to improve in the future, due to

the recent investment for the enhancement of the Algerian and Egyptian seismic networks. Unfortunately, at the time the present model is developed, such data are not yet publicly available.

12 Data and resources

Technical documentation and calculation results for the North Africa hazard model are available at https://www.globalquakemodel.org/gem as part of the Global Earthquake Hazard and Risk Model developed by the GEM Foundation. Calibration data and implementation information are available upon direct request to GEM foundation (hazard@globalquakemodel.org).

Acknowledgments

References

Abdunaser KM, McCaffrey KJW (2015) Tectonic history and structural development of the Zallah-Dur al Abd Sub-basin, western Sirt Basin, Libya. Journal of Structural Geology 73:33–48

Adly A, Poggi V, Fäh D, Hassoupa A, Omranb A (2017) Combining active and passive seismic methods for the characterization of urban sites in Cairo, Egypt. Geophys. J. Int. 210(1):428-442

Albini P, Musson RMW, Rovida A, Locati M, Gomez Capera AA, Viganò D (2014) Earthquake spectra 30(2):607-624

Al-Heety E A and Eshwehdi A (2006) Seismicity of the Northwestern Region of Libya: An Example of Continental Seismicity. Seismological Research Letters 77 (6):691-696

Álvarez-Gómez JA (2014) FMC: a one-liner Python program to manage, classify and plot focal mechanisms. Geophysical Research Abstracts, Vol. 16, EGU2014-10887.

Aki K, Richards P (1980). Quantitative Seismology, Theory and Methods, Vol. I and II. W.H. Freeman, San Francisco

Akkar S, Sandikkaya MA, Bommer JJ (2014) Empirical ground-motion models for point- and extendedsource crustal earthquake scenarios in Europe and the Middle East. Bull Earthq Eng 12:359–387

Ambraseys NN (1962) The seismicity of Tunis. Annals of Geophysics, 15:233–244

Ambraseys NN (1981) The El Asnam (Algeria) earthquake of 10 October 1980; conclusions drawn from a field study. Quarterly Journal of Engineering Geology and Hydrogeology 14:143–148

Ambraseys NN, Melvilie CP, Adam RD (1994). The seismicity of Egypt, Arabia and the Red Sea a historical review. Cambridge University Press, UK, 1–137

Arboleya ML, Teixell A, Charroud M and Julivert M (2004) A structural transect through the High and Middle Atlas of Morocco. Journal of African Earth Sciences, 39:319–327

Argus DF , Gordon RG, De Mets C, Stein S (1989) Closure of the Africa-Eurasia-North America plate Motions circuit and tectonics of the Gloria fault. J. of geophys. Resea., 94:5585-5602

Atkinson GM, Bommer JJ and Abrahamson NA (2014) Alternative Approaches to Modeling Epistemic Uncertainty in Ground Motions in Probabilistic Seismic-Hazard Analysis. Seismological Research Letters 85:1141–1144

Atkinson G and Boore D (2006) Earthquake ground-motion prediction equations for eastern North America. Bull Seismol Soc Am 96:2181–2205

Badawy A (2005) Present-day seismicity, stress field and crustal deformation of Egypt. J. Seismol. 9(2):267–276

Badawy A, Korrat I, El-Hadidy M, Gaber H (2016) Update earthquake risk assessment in Cairo, Egypt. Journal of Seismology 21(4):571-589

Ben Ayed N (1993) Evolution tectonique del'Avant-pays dela chaine alpine de Tunisie du debut du Mésozoique a l'Actuel, Annale des Mines et de la Geologie de Tunisie 32:286

Benouar D (1993) The seismicity of Algeria and adjacent regions during the twentieth century, PhD Thesis, Civil Engineering Department, Imperial College, University of London, pp. 712.

Benouar D (1994) Materials for the Investigation of the Seismicity of Algeria and Adjacent Regions, Annali Di Geofisica XXXVII (4)

Benouar D and Laradi N (1996) A Reappraisal of the Seismicity of the Maghreb Countries - Algeria, Morocco, Tunisia. Natural Hazards, 13(3):275-296

Benouar D, Molas GL, Yamazaki F (1996) Earthquake hazard mapping in the Maghreb countries -Algeria, Morocco, Tunisia- EarthquakeEngineering & Structural Dynamics Journal, 25(10):1151-1164

Bosworth W, Taviani M (1996) Late Quaternary reorientation of stress field and extension direction in the southern Gulf of Suez, Egypt: Evidence from uplifted coral terraces, mesoscopic fault arrays, and borehole breakouts. Tectonics 15:791–802

Bouhadad Y, Laouami N (2002) Earthquake hazard assessment in the western of Algeria, Journal natural hazards, 26:227-243

Bouaziz S, Barrier E, Soussi M, Turki MM, Zouari H (2002) Tectonic evolution of the northern African margin in Tunisia from paleostress data and sedimentary record. Tectonophysics 357:227–253

BSSC (2003) The 2003 NEHRP Recommended provisions for new buildings and other structures. Part 1: provisions (FEMA 450), Building Seismic Safety Council. www.bssconline.org

CEN (2004) Eurocode 8: design of structures for earthquake resistance—part 1: general rules, seismic actions and rules for buildings. European Committee for Standardization, British Standard BS EN 1998-1:2004: E, 219

Cornell C.A. (1968) Engineering Seismic Risk Analysis, Bulletin of the Seismological Society of America, 58(5):1583–1606

De Mets CR, Gordon RG, Argus DF and Stein S (1990) Current plate motions, Geophy. J. Inter., 101:425–478.

Di Giacomo D, Bondár I, Storchak D, Engdahl E R, Bormann P, Harris J (2015) ISC-GEM: Global Instrumental Earthquake Catalogue (1900–2009), III. Re-computed MS and mb, proxy MW, final magnitude composition and completeness assessment. Physics of the Earth and Planetary Interiors, 239:33–47

Di Giacomo D, Engdahl ER and Storchak DA (2018) The ISC-GEM Earthquake Catalogue (1904–2014): status after the Extension Project, Earth Syst. Sci. Data, 10:1877-1899

Campbell A (1968) The Barce (Al Marj) earthquake of 1963, In: Geology and Archaeology of Northern Cyrenaica, Libya. Petroleum Exploration Society of Libya 10th Annual Field Conference (pp. 183-195). Libya: F. T. Barr.

Chen Y-S, Weatherill G, Pagani M, Cotton F (2018) A transparent and data-driven global tectonic regionalization model for seismic hazard assessment. Geophysical Journal International, 213(22):1263–1280

Cherkaoui T-E, El Hassani A (2012) Seismicity and Seismic hazard in Morocco. Bulletin de l'Institut Scientifique, Rabat, section Sciences de la Terre. 34:45–55

Chiou BS-J, Youngs RR (2014) Update of the chiou and youngs NGA model for the average horizontal component of peak ground motion and response spectra. Earthq Sp 30:1117–1153

Cotton F, Scherbaum F, Bommer JJ, Bungum H (2006) Criteria for selecting and adjusting ground motion models for specific target regions: application to central Europe and rock sites. J Seismol 10:137–156

CRAAG (1994). Centre de Recherche en Astronomie Astrophysique et de Geophysique 1994. Les séismes en Algerie de 1365 à 1992. CRAAG. Report, Algiers.

Danciu L, Şeşetyan K, Demircioglu M, Gülen L, Zare M, Basili R, Elias A, Adamia S, Tsereteli N, Yalçın H, et al. (2017) The 2014 Earthquake Model of the Middle East: seismogenic sources. Bull Earthquake Eng. 16:1–32

Douglas J (2003). Earthquake ground motion estimation using strong-motion records: a review of equations for the estimation of peak ground acceleration and response spectral ordinates, Earth Sci. Rev. 61:43–104

El-Sayed A, Wahlström R, Kulhánek O (1994) Seismic hazard of Egypt. Nat Hazard 10(3):247–259

Ekstrom G, Nettles M, Dziewonski AM (2012) The global CMT project 2004–2010: centroid-moment tensors for 13,017 earthquakes. Phys Earth Planet Inter 200–201:1–9

Ezzelarab M, Shokry MMF, Mohamed AME, Helal AMA, Mohamed AA and El-Hadidy MS (2016) Evaluation of seismic hazard at the northwestern part of Egypt. Journal of African Earth Sciences, 113:114-125

Field EH, Jordan TH, Cornell CA (2003) OpenSH - A developing Community-modeling environment for seismic hazard analysis. Seismol Res Lett 74:406–419

Frankel A (1995). Mapping seismic hazard in the Central and Eastern United States. Seismological Research Letters 66(4):8-21

Giardini D. (ed) (1999) The Global Seismic Hazard Assessment Program 1992-1999. Annali Geofis., 42(6), 248 pp.

Giardini D, Danciu L, Erdik M, Sesetyan K, Demircioglu M, Akkar S, Gülen L and Zare M (2016) Seismic Hazard Map of the Middle East, doi:10.12686/a1

Gomez F, Barazangi M, Bensaid M (1996) Active tectonism in the intracontinental Middle Atlas Mountains of Morocco: synchronous crustal shortening and extension. Journal of the Geological Society 153:389–402.

Grünthal, G, Wahlström, R (2012) The European-Mediterranean Earthquake Catalogue (EMEC) for the last millennium. - Journal of Seismology, 16(3):535-570

Jiménez MJ, García-Fernández M and the GSHAP Ibero-Maghreb Working Group (M. Chadi, D. El Foul, A. Izquierdo, J.M. Martinez-Solares, C. Sousa-Oliveira, B.A. Tadili) (1999) Seismic hazard assessment in the IberoMaghreb Region. Annali Geofis., 42:1057-1066

Jiménez-Munt I, Fernàndez M, Torne M and Bird P (2001). The transition from linear to diffuse plate boundary in the Azores- Gibraltar region: results from a thin-sheet model. Earth Planet. Sci. Lett., 192:175-189

Hanks TC and Kanamori H. (1979) A moment magnitude scale, Journal of Geophysical Research, 84(5):2348 - 2350

Hamdache M, Peláez JA, Talbi A, López Casado C (2010a) A unified catalog of main earthquakes for Northern Algeria from A.D. 856 to 2008. Seismol. Res. Lett., 81: 732-739

Hamdache M, Peláez JA, Talbi A, Mobarki M (2010b) Evaluation of probabilistic seismic hazard in Northern Algeria. A contribution to the Algerian building code. 5ème Symposium International sur la Construction en Zone Sismique. 26-27 octubre, 2010. Chlef, Argelia.

Hamdache M, Peláez JA, Talbi A, Mobarki M and López Casado C (2012) Ground motion hazard values for Northern Algeria. Pure and Applied Geophysics, 169:711–723

Hassen A (1983) Seismicity of Libya and related problems. PhD Thesis. Department of civil Engineering, Colorado State University, Colorado.

Hussein HM, Abou Elenean KM, Marzouk IA, et al (2013) Present-day tectonic stress regime in Egypt and surrounding area based on inversion of earthquake focal mechanisms. Journal of African Earth Sciences 81:1–15

IASPEI (2013) Summary of Magnitude Working Group recommendations on standard procedures for determining earthquake magnitudes from digital data. (http://www.iaspei.org/commissions/commission-on-seismological-observation-and-interpretation/Summary_WG_recommendations_20130327.pdf)

Kagan YY (2005) Double-couple earthquake focal mechanism: random rotation and display. Geophysical Journal International 163:1065–1072

Kariche J, Meghraoui M, Ayadi A, Boughacha M-S (2017) Stress Change and Fault Interaction from a Two Century-Long Earthquake Sequence in the Central Tell Atlas, AlgeriaStress Change and Fault Interaction from a Two Century-Long Earthquake Sequence. Bulletin of the Seismological Society of America 107:2624–2635

Kaverina AN, Lander AV, Prozorov AG (1996) Global creepex distribution and its relation to earthquake-source geometry and tectonic origin. Geophysical Journal International 125(1):249–265

Kebeasy R (1980) Seismicity and seismotectonics of Libya. In The Geology of Libya. Vol. 3. Eds. M. J. Salem and M. T. Busrewil, 955–963. London: Academic Press.

Ksentini A, Romdhane NB (2014) Updated seismic hazard assessment of Tunisia. Bulletin of Earthquake Engineering, 12(2):647-670

Lagesse R, Free M, Lubkowski Z (2017) Probabilistic seismic hazard assessment for Libya, 16th World Conference on Earthquake, 16WCEE. Santiago Chile, January 9th to 13th.

Leonard M (2010). Earthquake fault scaling: Self-consistent relating of rupture length, width, average displacement, and moment release, Bull. Seismol. Soc. Am., 100(5A):1971–1988

Leonard M (2014). Self-consistent earthquake fault-scaling relations: Update and extension to stable continental strike-slip faults, Bull. Seismol. Soc. Am., 104:1971–1988

Mahmoud S, Reilinger R, McClusky S, Vernant P and Tealeb A (2005) GPS evidence for northward motion of the Sinai block: Implications for E. Mediterranean tectonics, Earth Planet. Sci. Lett., 238:217–224

Maouche S, Meghraoui M, Morhange C, et al (2011) Active coastal thrusting and folding, and uplift rate of the Sahel Anticline and Zemmouri earthquake area (Tell Atlas, Algeria). Tectonophysics 509:69–80

Mauffret A (2007) The Northwestern (Maghreb) boundary of the Nubia (Africa) Plate. Tectonophysics 429:21–44

McGuire RK (2004) Seismic Hazard and Risk Analysis. Oakland: Earthquake Engineering Research Institute, MNO-10.

Medina F, Bensaid I and Tangi A (2011) Catalogue of Focal Mechanisms of Moroccan Earthquakes for the Period 1959-2007; Analysis of Parameters. Bulletin de l'Institut Scientifique, Rabat, Section Sciences de la Terre, 33:37-46

Meghraoui M, Cisternas A and Philip H (1986) Seismotectonics of the lower Chéliff basin: Structural background of the El Asnam (Algeria) earthquake, Tectonics, 5(6):809-836.

Meghraoui M, Outtani F, Choukri A, De Lamotte DF (1999) Coastal tectonics across the South Atlas thrust front and the Agadir active zone, Morocco. Geological Society, London, Special Publications 146:239–253

Meghraoui M, Philip H, Albarede F, Cisternas A (1988) Trench investigations through the trace of the 1980 El Asnam thrust fault: Evidence for paleoseismicity. Bulletin of the Seismological Society of America 78:979–999

Meghraoui M, Pondrelli S (2013) Active faulting and transpression tectonics along the plate boundary in North Africa. Annals of Geophysics 55:. https://doi.org/10.4401/ag-4970

Meghraoui M (1988) Géologie des zones sismiques du nord de l'Algérie, Tectonique active, Paléosismologie et synthèse sismotectonique, PhD Thesis, Univ. Paris-Sud Orsay, 350 pp.

Mekkawi M, Schnegg P-A, Arafa-Hamed T, Elathy E (2005) Electrical structure of the tectonically active Kalabsha Fault, Aswan, Egypt. Earth and Planetary Science Letters 240:764–773

Mejri L, Regard V, Carretier S, Brusset S, Dlala M (2010). Evidence of Quaternary active folding near Utique (Northeast Tunisia) from tectonic observations and a seismic profile. Comptes Rendus Geoscience. 342(11):864-872

Mourabit T, Abou Elenean KM, Ayadi A, Benouar D, Ben Suleman A, Bezzeghoud M, Cheddadi A, Chourak M, ElGabry MN, Harbi A, Hfaiedh M, Hussein HM, Kacem J, Ksentini A, Jabour N, Magrin A, Maouche S, Meghraoui M, Ousadou F, Panza GF, Peresan A, Romdhane N, Vaccari F and Zuccolo E, (2014). Neo-deterministic seismic hazard assessment in North Africa. Journal of seismology, 18(2):301-318

Ouyed M, Yielding G, Hatzfeld D and King GCP (1983) An aftershock study of the El Asnam (Algeria) earthquake of 1980 October 10, Geophys. J.R. astr. Soc. 73:605–639

Pagani M, Monelli D, Weatherill G, Danciu L, Crowley H, Silva V, Henshaw P, Butler L, Nastasi M, Panzeri L, Simionato M, Vigano D (2014) OpenQuake-engine: an open hazard (and risk) software for the global earthquake model. Seismol Res Lett 85:692–702

Pagani M, Garcia-Peláez J, Gee R, Johnson KL, Poggi V, Silva V, Simionato M, Styron RH, Viganò D, Danciu L, Monelli D, Weatherill G (2020) The 2018 version of the Global Earthquake Model: Hazard component. Accepted for publication in Earthquake Spectra

Paradise TR (2005) Perception of earthquake risk in Agadir, Morocco: A case study from a Muslim community. Global Environmental Change Part B: Environmental Hazards 6:167–180

Patriat P, Segoufrin J, Schlich R, Goslin J, Auzende JM, Benzart P, Bonnin J, and Olivet JL (1982) Les mouvements relatifs de l'Inde, de l'Afrique et de l'Eurasie, Bull. Soc. Geol. Fr. 24(2):363-373

Pastor Castilla À, Teixell A, Arboleya ML (2013) Rates of Quaternary deformation in the Ouarzazate Basin (Southern Atlas Front, Morocco). Ann Geophys 55:. https://doi.org/10.4401/ag-4940

Peláez JA, Hamdache M and López Casado C (2003). Seismic hazard in northern Algeria using spatially smoothed seismicity. Tectonophysics 372:105-119

Peláez JA, Hamdache M and Casado CL (2006) Seismic Hazard in Term of Spectral Accelerations and Uniform Hazard Spectra in Northern Algeria. Pure Appl. Geophys., 163:119-135

Peláez JA, Chourak M, Tadili BA, Aït Brahim L, Hamdache M, López Casado C, Martínez Solares JM (2007) A Catalog of Main Moroccan Earthquakes from 1045 to 2005. Seismological Research Letters, 78(6):614-621

Peláez, José, Henares, J, Hamdache M, Sanz de Galdeano C (2018). A Seismogenic Zone Model for Seismic Hazard Studies in Northwestern Africa. 10.1007/978-3-319-77359-9_29.

Perez ND, Teixell A, Gómez-Gras D, Stockli DF (2019) Reconstructing Extensional Basin Architecture and Provenance in the Marrakech High Atlas of Morocco: Implications for Rift Basins and Inversion Tectonics. Tectonics 38:1584–1608

Pezeshk S, Zandieh A, Tavakoli B (2011) Hybrid empirical ground-motion prediction equations for eastern North America using NGA models and updated seismological parameters. Bull Seismol Soc Am 101:1859–1870

Poggi V, Durrheim R, Mavonga Tuluka G, Weatherill G, Gee R, Pagani M, Nyblade A, Delvaux D (2017) Assessing Seismic Hazard of the East African Rift: a pilot study from GEM and AfricaArray. Bulletin of Earthquake Engineering. 15(11): 4499–4529

Poggi V, Edwards B and Fäh D (2018) Development of hazard- and amplification-consistent elastic design spectra. Soil Dynamics and Earthquake Engineering, Special Issue "Seismic ground response and site effects: From theoretical and experimental studies to design codes". 128:1-16

Rigby M (2008) Recent faulting and active shortening of the Middle Atlas Mountains, Morocco, within the diffuse African-Eurasian Plate boundary. University of Missouri-Columbia

Said R (1981) The geological evolution of the River Nile. Springer-Verlag, New York Inc, U.S.A, p. 151.

Saïd A, Baby P, Chardon D, Ouali J (2011) Structure, paleogeographic inheritance, and deformation history of the southern Atlas foreland fold and thrust belt of Tunisia. Tectonics 30:TC6004. https://doi.org/10.1029/2011TC002862

Sawires R, Peláez J, Fat-Helbary RE, Ibrahim HA and García-Hernández MT (2015) An updated seismic source model for Egypt. Earthquake engineering-from engineering seismology to optimal seismic design of engineering structures. InTech. ISBN, 978-953.

Schwartz DP and Coppersmith KJ (1984). Fault Behaviour and Characteristic Earthquakes: Examples from the Wasatch and San Andreas fault zones. In: Journal of Geo- physical Research 89.B7:5681–5698

Sébrier M, Siame L, Zouine EM, et al (2006) Active tectonics in the Moroccan High Atlas. Comptes Rendus Geoscience 338:65–79

Serpelloni E, Vannucci G, Pondrelli S, et al (2007) Kinematics of the Western Africa-Eurasia plate boundary from focal mechanisms and GPS data. Geophys J Int 169:1180–1200

Sharp IR, Gawthorpe RL, Underhill JR, Gupta S (2000). Fault propagation folding in extensional settings: examples of structural style and syn-rift sedimentary response from the Suez Rift, Egypt. Geological Society of America Bulletin 112:1877–1899

Soumaya A, Ben Ayed N, Delvaux D, Ghanmi M (2015) Spatial variation of present-day stress field and tectonic regime in Tunisia and surroundings from formal inversion of focal mechanisms: Geodynamic implications for central Mediterranean. Tectonics 34:2015TC003895. https://doi.org/10.1002/2015TC003895

Storchak DA, Di Giacomo D, Bonda´r I, Engdahl ER, Harris J, Lee WHK, Villasen˜or A, Bormann P (2013) Public Release of the ISC-GEM Global Instrumental Earthquake Catalogue (1900-2009). Seismol Res Lett 84:810–815

Storchak DA, Di Giacomo D, Engdahl ER, Harris J, Bonda´r I, Lee WHK, Bormann P, Villasen˜or A (2015) The ISC-GEM global instrumental earthquake catalogue (1900–2009). Introd Phys Earth Planet Int 239:48–63

Storchak DA, Harris J, Brown L, Lieser K, Shumba B, Verney R, Di Giacomo D, Korger EI M (2017). Rebuild of the Bulletin of the International Seismological Centre (ISC), part 1: 1964–1979. Geosci. Lett. (2017) 4:32. doi: 10.1186/s40562-017-0098-z

Suleiman AS, Albini P and Migliavacca P (2004) A short introduction to historical earthquakes in Libya, Ann. Geophys., 47(2/3):545–554

Vilanova SP, Nemser ES, Besana-Ostman GM, Bezzeghoud M, Borges JF, Da Silveira AB, Cabral J, Carvalho J, Cunha PP, Dias RP, Madeira J, Lopes FC, Oliveira CS, Perea H, Garcı´a-Mayordomo J, Wong I, Arvidsson R, Fonseca JFBD (2014) Incorporating descriptive metadata into seismic source zone models for seismic-hazard assessment: a case study of the Azores-West Iberian region. Bull Seismol Soc Am 104:1212–1229

Vogt J (1993) Further research on the historical seismicity of Tunisia. Terra Nova 5:475–476

Weatherill GA, Pagani M and Garcia J (2016) Exploring earthquake databases for the creation of magnitude-homogeneous catalogues: tools for application on a regional and global scale. Geophys. J. Int., 206(3):1652-1676

Woessner J, Danciu L, Giardini D, Crowley H, Cotton F, Grünthal G et al (2015): The 2013 European seismic hazard model: key components and results. Bull Earthq Eng 13(12):3553–3596

Youngs RR and Coppersmith KJ (1985) Implications of fault slip rates and earth- quake recurrence models to probabilistic seismic hazard estimates. In: Bulletin of the Seismological Society of America, 75:939–964

Tables

Table 1 Main characteristics of the catalogue sources used in this study. The values correspond to the events within the buffer region selected for North Africa (see **Figure 1**)

Catalogue	Covered Period	Magnitude Range	No. Events
ISC-GEM	1927 – 2012	5.5 – 7.8	65
ISC-REV	1910 – 2013	0.7 – 8.1	11428
GCMT	1977 – 2013	4.7 - 7.2	97
IGN	1393 – 2017	-2.0 – 7.3	81396
EMEC	1016 – 2006	4.0 – 8.7	3699
GEM-GHEC	1033 – 1891	6.0 – 8.5	25

Table 2 Comparison between total number of hypocentral location solutions (subdivided per agency) and Prime solutions from the ISC-Review bulletin within the investigated region.

	Agency (Number of available location solutions > 10)
All Solutions	ISC (9321), MDD (6951), NEIC (4991), CSEM (3847), INMG (2320), LDG (2273), ISCJB (1707), IPRG (1386), CNRM (1330), IDC (1210), IGIL (1131), JSO (1070), CRAAG (1020), LIS (877), SFS (762), MOS (728), ATH (691), EHB (553), NEIS (526), NAO (507), SPGM (456), GII (443), RYD (433), HLW (432), EIDC (423), HFS (373), BJI (348), BCIS (343), RBA (297), STR (292), ROM (265), LAO (234), NIC (199), ISK (189), NSSC (187), THE (180), GRAL (169), USCGS (131), SNSN (127), MED_RCMT (123), HFS2 (115), SGS (113), IASPEI (109), IAG (108), TUN (101), ZUR_RMT (97), PDG (90), DDA (81), HRVD (78), SZGRF (72), ISS (54), HFS1 (54), PEK (52), ZUR (42), DUSS (40), CENT (39), GCMT (35), GUTE (31), BER (27), CGS (25), PDA (25), BGS (24), PTO (23), TTG (23), BEO (11), TEH (10)
Prime Selection	ISC (9321), MDD (1025), IPRG (207), IDC (123), CRAAG (97), CSEM (85), INMG (81), JSO (62), HLW (61), RYD (52), CNRM (37), SPGM (37), ROM (33), GUTE (29), LIS (25), TUN (24), BCIS (22), LAO (16), RBA (14), NEIC (13), SGS (10), GII (10)

Table 3 Size of time and spatial windows used to identify potentially duplicate events when comparing and merging earthquake catalogues. Windows have different length depending on the analysed period.

	Historical (<1900)	Pre-instrumental (1900-1963)	Instrumental (>1963)
Δt	2 day	10 minute	120 second
Δd	150 km	100 km	50 km

Table 4 Comparison between total number of events available from each earthquake catalogue, and the number of events after duplicate finding and location solution selection.

	ISC-GEM	ISC-Rev	GCMT	IGN	EMEC	GEM-GHEC
Total	67	10,429	101	6,840	3,782	25
Selection	67	10,374	3	1,817	1,960	5

Table 5 Magnitude agency selection rules, sorted within groups of magnitude types, from high to low priority. In bold are the catalogue data, while with normal font are ISC reported solutions. Magnitude types are named according to IASPEI recommendations (for further details, please refer to the IASPEI Working Group on Magnitudes, 2013).

Group	Agency (Magnitude type)
Reference (Mw)	**GCMT-NDK**, GCMT, HRVD, NEIC, HRVD-NEIC, USGS-NEIC, **IGN**, CSEM, IPRG, GII, NIC, IAG, MED_RCMT, ZUR_RMT, **ISC-GEM**
Reliable types (Ms and mb)	ISC (MS, Ms), IDC (MS), NEIC (MS, MSZ, Ms), NEIS (MS), CSEM (Ms), ISC (mb), IGN (mb), NEIC (mb), NEIS (mb), CSEM (mb), USCGS (mb), MDD (mb)
Less-reliable types (mb, ML)	IDC (mb, mb1), IPRG (mb), GII (mb), IPRG (mL), CSEM (ML), GII (ML), CNRM (ML)
Converted Mw	**GEM-GHEC** (Mw, Ms, mb), **EMEC** (Mw)
Poorly calibrated agencies	IGN (MbLg, mbLg, MDs), JSO (ML, mL), MDD (MD), CNRM (MD), JSO (MD), LIS (MD), RYD (MD, md), HLW (Ml), LDG (Ml, mL), ATH (MD), RBA (md)

Table 6 Conversion rules used to convert different magnitude types into M_W. Events outside the range of applicability of the rule have been discarded.

Type	Mw Conversion rule	Range
Ms (MS, MSZ)	Bilinear - Weatherill et al. (2016)	$3.5 \leq M \leq 8.0$
mb (mb1)	Linear - Weatherill et al. (2016)	$3.5 \leq M \leq 7.0$
ML (Ml, mL, MbLg, mbLg)	Polynomial – Edwards et al. (2016)	$M \leq 6.0$
MD (md)	1:1 conversion	--

Table 7 Seismicity parameters of the North Africa source zonation model. M^{max} is calculated as the maximum observed magnitude in each zone plus 0.5.

Group	Source	*a*-value	*b*-value	M^{max} (M^{obs}+0.5)
1 - High / Middle Atlas	1	4.31	1.10	6.9
	2	4.08		6.9
	3	4.39		7.2
	4	4.01		5.7
	5	4.45		6.9
	6	4.08		5.8
	7	3.92		6
	8	4.09		6.3
	9	4.22		6.11
	10	4.15		5.58
2 - Rif / Tell Atlas	11	4.09	0.98	7.8
	12	3.76		7.34
	13	4.47		7
	14	4.34		6.33
	15	3.89		6.3
	16	3.72		6.86
	17	4.11		7.6
	18	4.12		7.5
3 - West Algeria / Tunisia	19	3.64	0.93	6.5
	20	3.41		6.3
	21	3.83		5.83
	22	3.81		6.3
	23	3.13		7.5

	24	3.39		6.3
4 - Dead Sea Fault Zone	25	3.67	0.99	7.71
	26	4.06		8.15
	27	3.37		5.3
5 - On-Shore Egypt / Red Sea	28	4.18	1.11	7.16
	29	4.12		6.7
	30	4.35		7.1
	31	4.27		5.4
	32	3.99		6.01
	33	3.72		6.33
6 - Off-Shore Egypt	34	3.42	0.96	6.13
	35	3.61		6.73
	36	3.27		6.38
	37	3.88		6.87
7 - Libya	38	4.27	1.13	7.3
	39	4.54		6.32
	40	4.25		5.3
	41	4.52		5.97
	42	4.09		6.4
8 - Iberia	43	4.00	1.07	7.2
	44	3.99		7
	45	4.23		7.3
	46	4.00		5.9
	47	3.95		7.2
	48	4.50		7.1
	49	3.83		6.6
	50	4.24		8.3
	51	4.75		9
	52	3.99		7.2
9 - Atlantic Off-Shore /	53	4.87	1.12	6.8
Canary Islands	54	4.74		5.75

Table 8 Source mechanism distribution parameters for each seismotectonics group of the North Africa source model.

Group	Prob.	Strike	Dip	Rake	Description
1	0.6	240	60	45	Combination of R and SS faults. SS (mostly LL) is
	0.4	240	45	90	dominant in the South, while R is more evident in the
					North.
2	0.4	240	60	135	Combination of R and SS faults. R is always dominant.
	0.4	240	45	90	SS is mostly LL in the West, RL in the East.
	0.2	240	60	45	
3	0.6	240	60	135	Combination of R and SS faults. SS (mostly RL) is
	0.4	240	45	90	dominant in the South, while R is more evident in the
					North.
4	0.5	20	90	0	Pure SS, considering both LL and RL.
	0.5	20	90	180	
5	0.4	300	60	-90	Mostly N faulting, with some contribution from RL
	0.4	120	60	-90	oblique slip faults.
	0.2	60	90	180	
6	0.4	60	90	180	Mostly N faulting, with some contribution from RL slip
	0.6	110	60	-90	faults.
7	0.4	110	90	180	Mixture of RL SS, pure R and N mechanisms.
	0.3	110	60	-90	
	0.3	110	45	90	
8	0.5	110	90	180	Pure LL SS according to the main fault mapped in the
	0.5	240	60	135	paper of Gonzalez. Likely the mechanism is similar
					along the whole offshore.
9	1	30	90	0	Pure LL SS (simplified)

R = reverse, N = normal, SS = strike slip; LL = left-lateral; RL = right-lateral

Table 9 Table summarizing parameters, their functions and the assumptions used for the definition of a fault source in the NAF model.

Parameters	Purpose	Assumption
Fault trace	Define 3D geometry of fault surface	
Upper seismogenic depth		Fixed at depth = 0
Lower seismogenic depth		Defined by applying Leonard (2014)
Dip angle		Following the Aki-Richards convention (Aki and Richards, 1980)
Rake angle	Defines faulting style	Following the Aki-Richards convention (Aki and Richards, 1980)
Magnitude-Frequency distribution (MFD)	Defines total moment rate and the relative frequency of earthquakes of different magnitude	Double-truncated Gutenberg-Richter (GR) distribution. Lower-bound magnitude fixed to M6.0 Upper-bound magnitude defined by applying Leonard(2014)
Magnitude-Area scaling relationship	Define sizes and shapes of rupture planes	Leonard (2014)
Rupture aspect ratio (length/width)		Fixed to 2.0

Table 10 Grouping of sources by tectonic similarity and weighting scheme for the GMPE logic-tree

Group ID	Type	Source Zone ID	CY	AK	AB	PZ
A	ASC	1, 2, 3, 11, 12, 13, 14, 15, 16, 17, 18, 19, 20, 22, 23, 24, 25, 26, 29, 30, 31, 32, 41, 43, 44, 45, 46, 47, 48, 49, 50, 51, 52	0.5	0.5	0	0
B	ASC/SCC	4, 5, 6, 7, 8, 9, 21, 27, 28, 36, 38, 39, 40	0.25	0.25	0.25	0.25
C	SCC	10, 33, 34, 35, 37, 42	0	0	0.5	0.5

The four selected ground motion prediction equations (CY Chiou and Youngs 2014; AK Akkar et al., 2014; AB Atkinson and Boore 2006; PZ Pezeshk et al., 2011) have been applied with different weight to each zone belonging to a specific tectonic group (A, B, C)

Figures
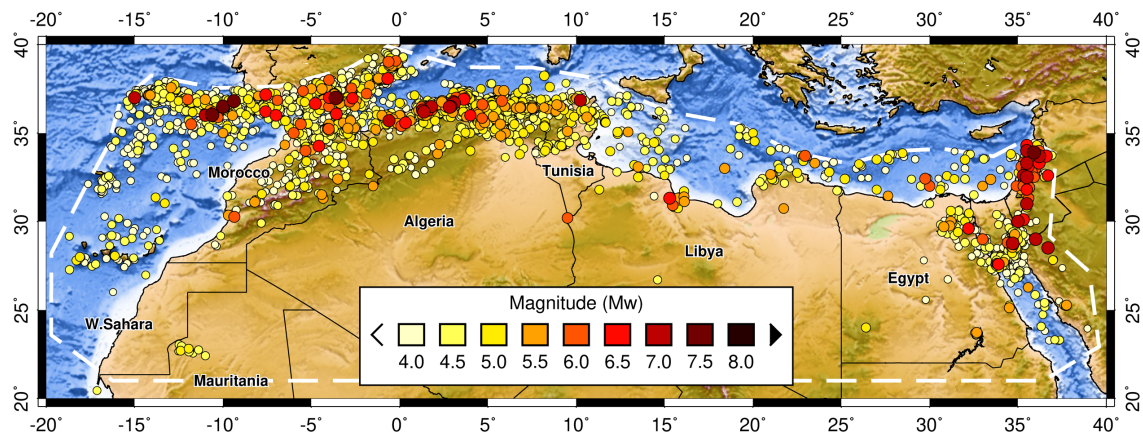
Figure 1 – The Mw homogenised earthquake catalogue for North Africa. Dashed polygon shows the investigation area.

(a)
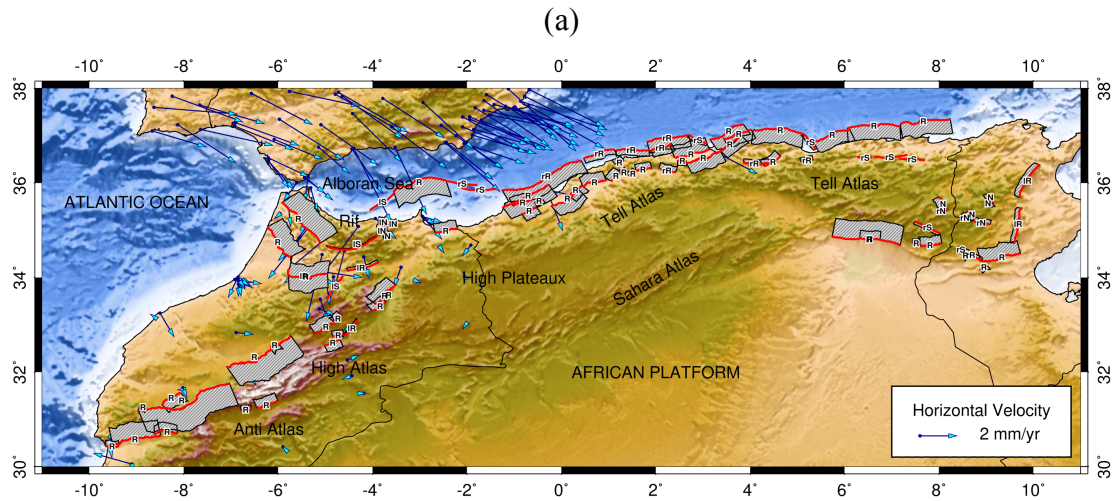
Figure 2 – Trace (in red) and surface projection (in gray) of the modelled active faults of the Maghreb (a) and Egypt (b) regions. Dominant mechanism is indicated with R (Reverse), N (Normal) or S (Strike-slip), while lateral and oblique slip components are indicated with l (left-lateral) and r (right-lateral). Measured GPS velocities are shown with blue arrows.

(b)
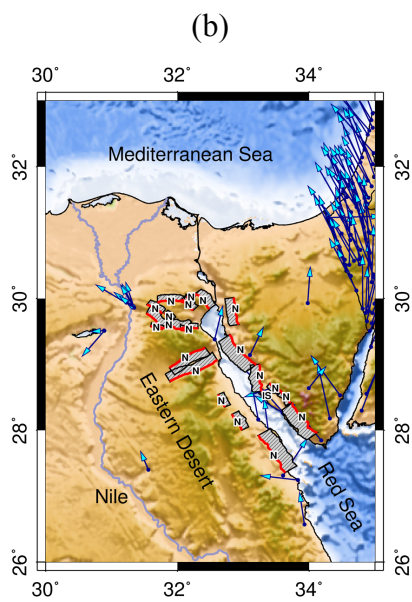
Figure 2 (Continue)
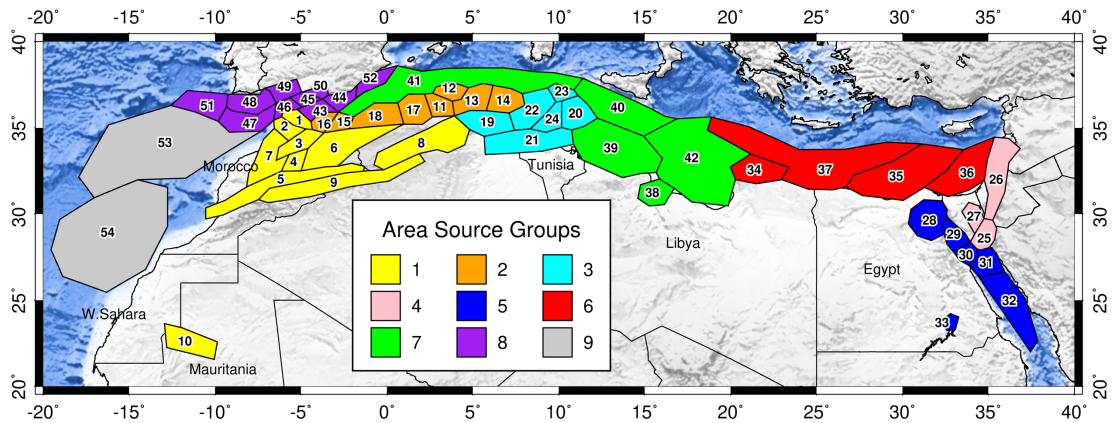
Figure 3 – The proposed source zonation for North Africa. Different colours are used to represent the 9 main tectonic groups (see Table 10) of the region.

Group 1)
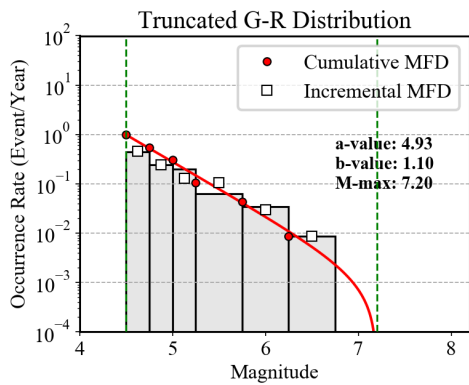
Group 2)
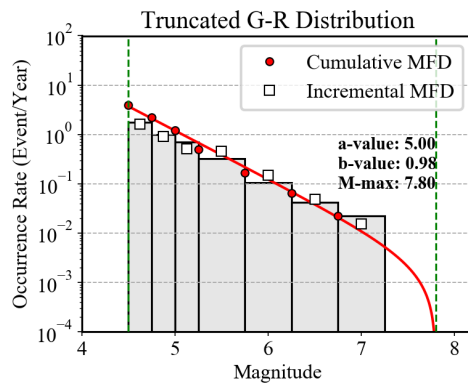
Group 3)
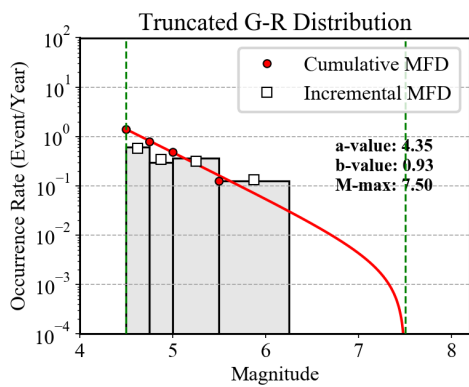
Group 4)
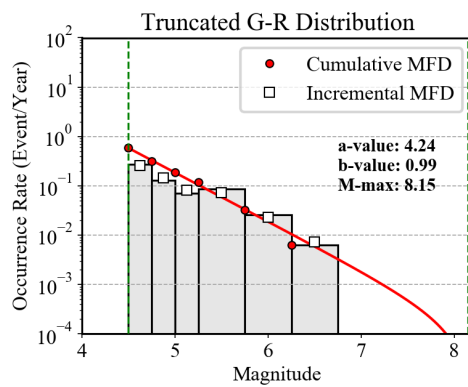
Group 5)
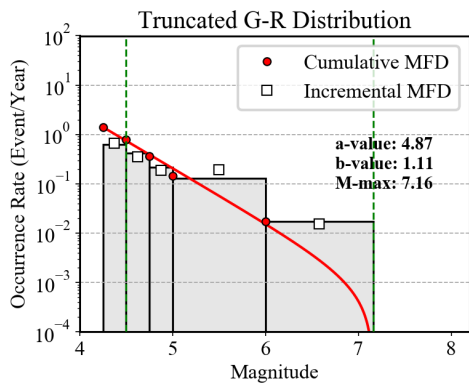
Group 6)
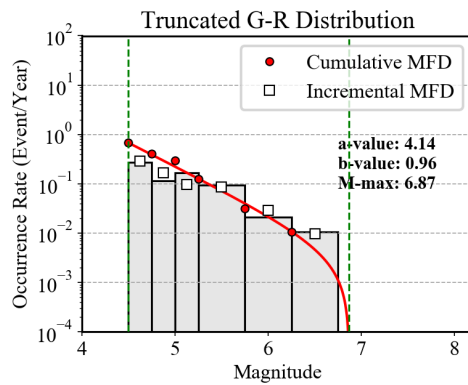
Group 7)
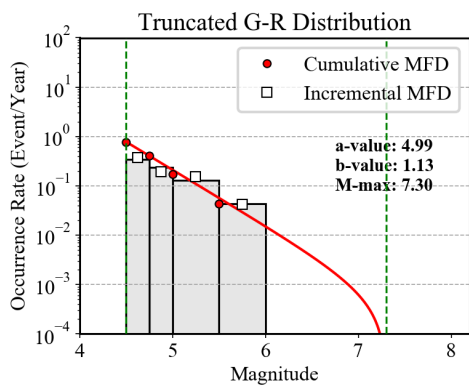
Group 8)
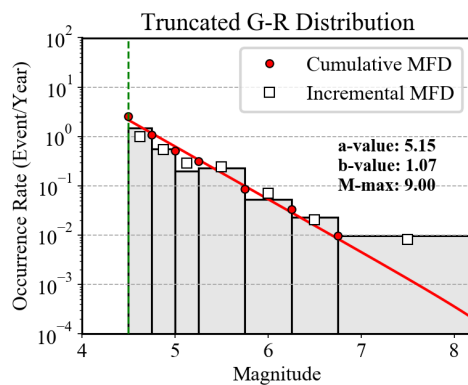
Figure 4 - Magnitude occurrence relations of the North Africa seismicity model for the first 8 tectonic groups. The double-truncated Gutenberg-Richter model is presented with red line for the cumulative rates and with grey histogram for the incremental (non-cumulative) rates; white squares indicate the reference magnitude of each occurrence bin. M^{max} is the largest from all source zones of each group.
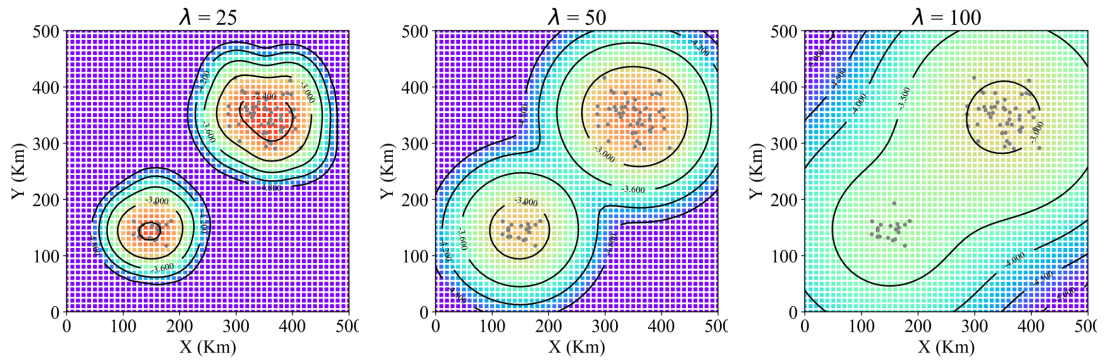
Figure 5 – Example of influence of λ on the redistribution of the earthquake rate (isolines) on a simple box area of 500km^2 based on spatial distribution of earthquake epicentres (grey dots).
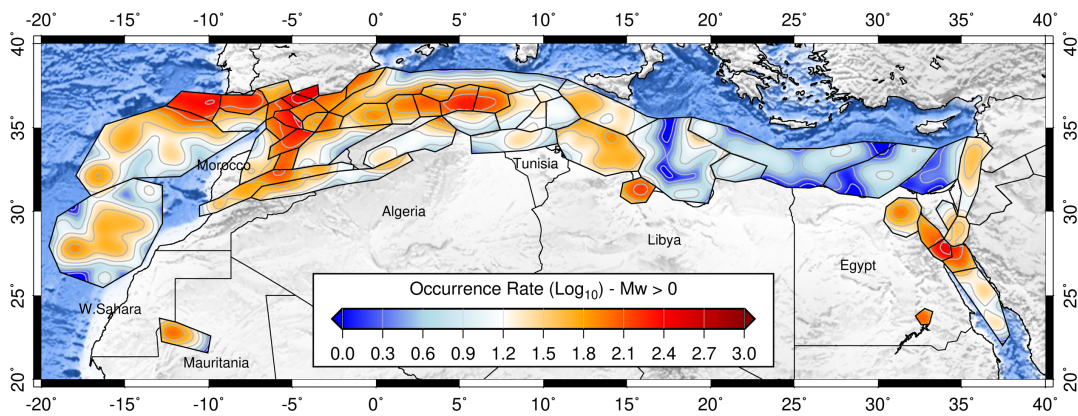
Figure 6 – Example of spatial redistribution of the cumulative annual rates (M>0) using a decay parameter (λ) of 50. Rates are intended by unit area of 0.1°x0.1° (about 11km^2).
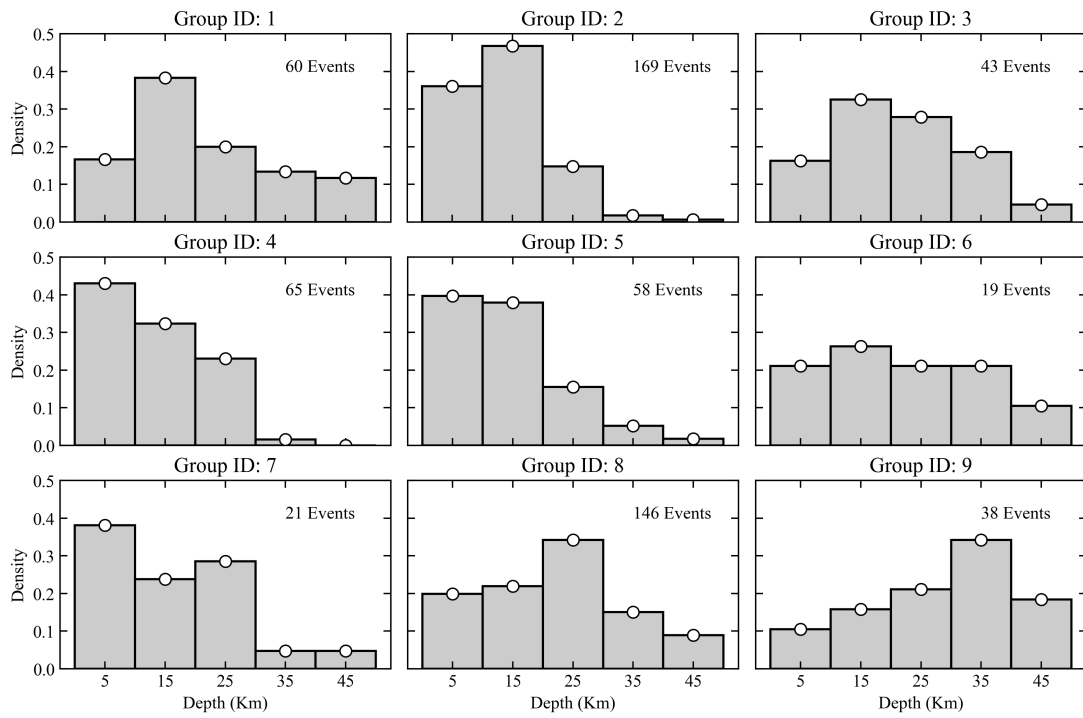
Figure 7 - Earthquake hypocentral depth distribution of the nine seismotectonics groups of the North Africa source model.
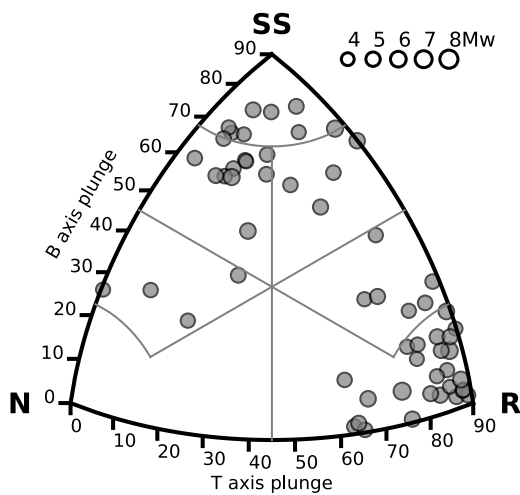
Figure 8 – Example of ternary diagram for the classification of the dominant rupture mechanism of zone 2.
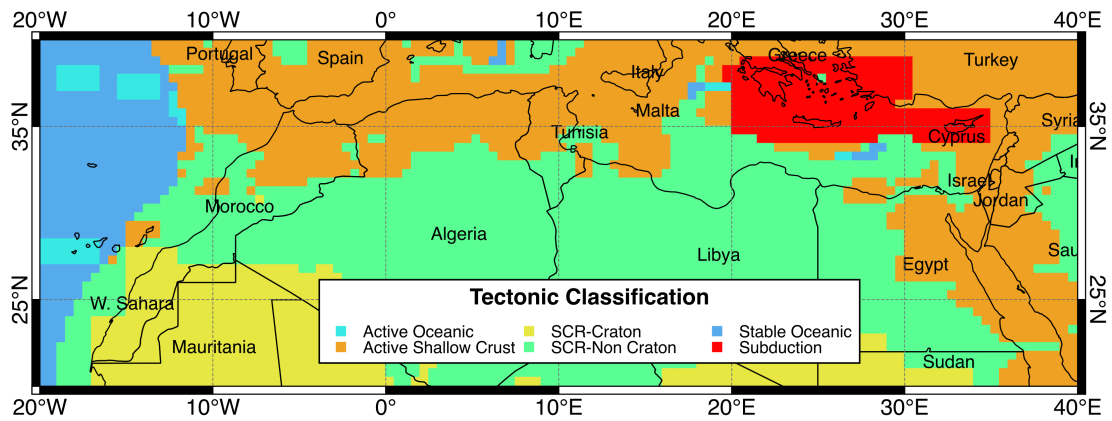
Figure 9 – Tectonic classification proposed by Chen et al. (2018) used to guide the regionalisation of the North Africa seismic source zones (see Table 10).
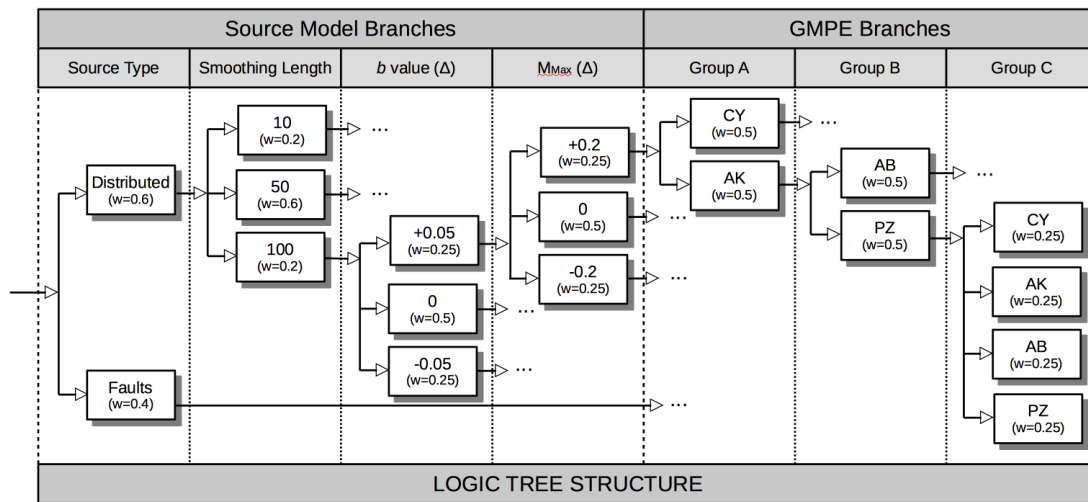

Figure 10 – Diagram representation of the logic-tree structure of the North Africa hazard Model. The implementation consists of 432 branches, distributed over 6 levels (3 for the GMPE and 3 for the source model).
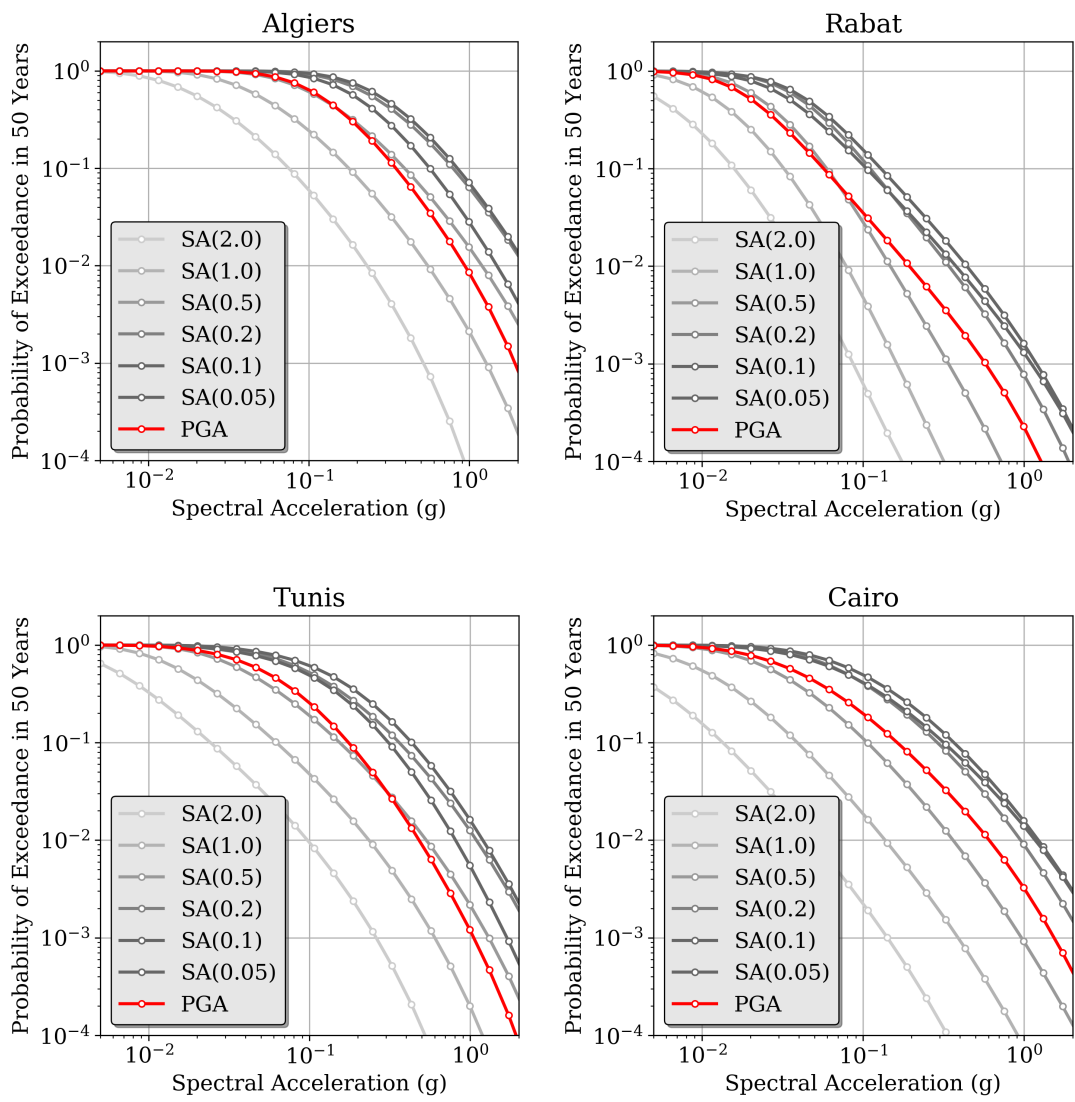
Figure 11 – Mean hazard curves computed at four selected capitals in North Africa. Calculations are made for PGA (in red) and for increasing spectral periods from 0.05s to 2s.
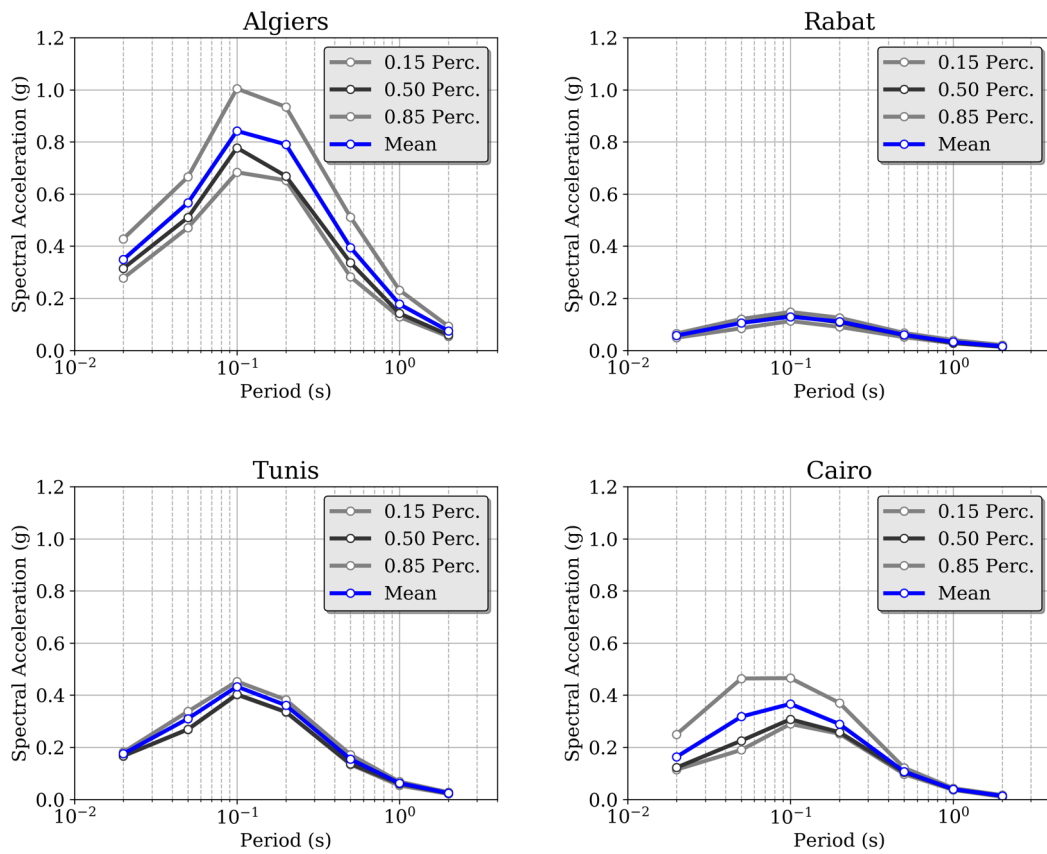
Figure 12 – Uniform Hazard Spectra (UHS) computed for 10% probability of exceedance in 50 years (equivalent to a return period of 475 year) at the four selected North African capitals as in Figure 11. Mean spectra (in blue) have systematically higher accelerations than the 0.5 percentile (in black), which highlight a certain skewness of the distribution of uncertainties.
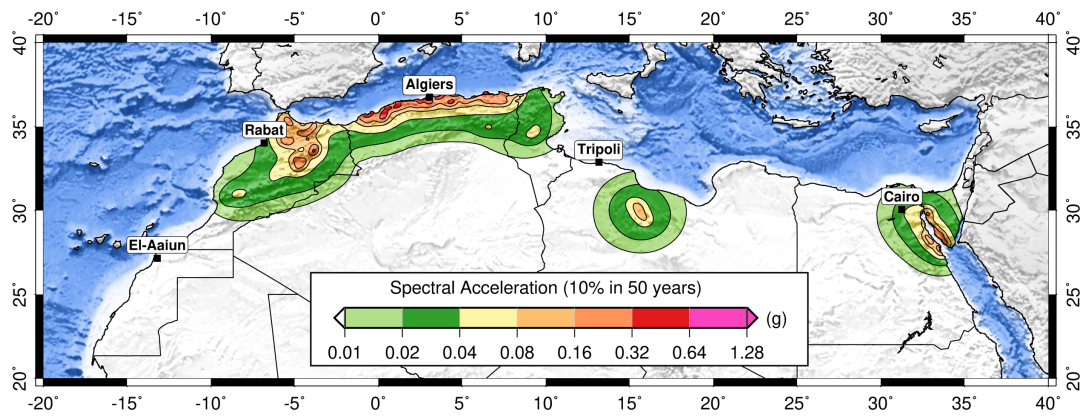
(a)
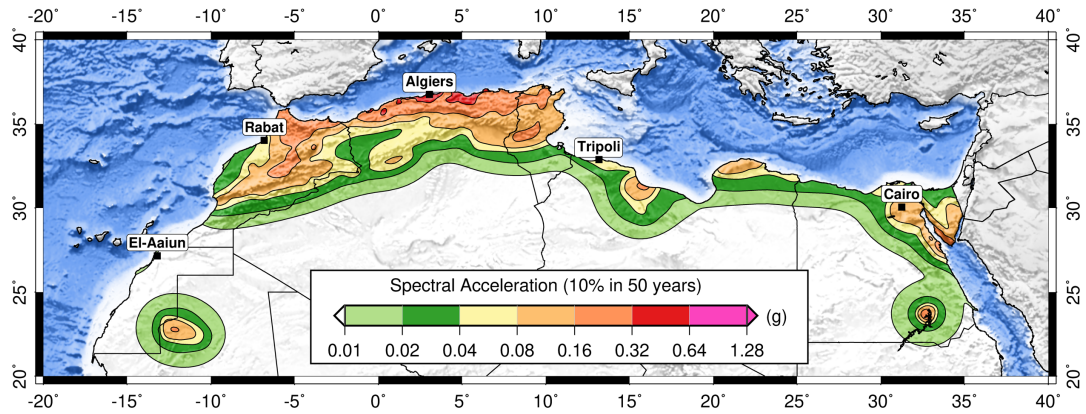
(b)

Figure 13 – Maps of spectral acceleration at PGA (g) calculated for 10% probability of exceedance in 50 years using the combined source models (a) and just using the fault model (b).